Environmental Science and Pollution Research (2023) 30:81647–81666
https://doi.org/10.1007/s11356-022-23217-z

MATERIALS FOR ENERGY CONVERSION AND ENVIRONMENTAL APPLICATIONS

Generation of red light with intense photoluminescence assisted by Forster resonance energy transfer from Znq_2 and DCM thin films

Amina Laouid[1,2,3] · Amine Alaoui Belghiti[2] · Krzysztof Wisniewski[1] · Abdelowahed Hajjaji[2] · Bouchta Sahraoui[4] · Anna Zawadzka[1,3]

Received: 3 April 2022 / Accepted: 19 September 2022 / Published online: 3 October 2022
© The Author(s) 2022

Abstract
In this work, a novel experimental investigation of photoluminescence properties of Znq_2 thin films co-doped with different concentrations of DCM were performed. The thin films were successfully deposited on glass substrates with different compositions, under high vacuum, by using the vacuum evaporation technique. For all compositions, the photoluminescence was measured at room temperature and also at low temperature in a wide range from 77 to 300 K with a step of 25 K in a high vacuum. The lifetime of the sample studied in real time was also measured using the decay time technique. The results obtained confirm that the doping influences the intensity of the DCM photoluminescence and also shows a complete energy transfer occurred from Znq_2 to DCM which may have shifted the photoluminescence peak from Znq_2 to the orange wavelength region which is related to DCM. The lifetime of the sample studied in real time was about 4.47 ns for Znq_2 and while all the other samples showed two decay time components. As a result, the doping influences the optical properties of Znq_2 and makes it a potential candidate for optoelectronic applications.

Keywords Photoluminescence · Decay time · Thin film · DCM · Znq_2 · Physical vapor deposition · AFM

Introduction

Organic materials have become among the major research topics lately (Data and Takeda 2019; Yu et al. 2021); its use has given rise to promising applications at the industrial scale and opened up new perspectives for fundamental physics (engineering at the molecular scale), because of their broad potential benefits in various fields such as optoelectronics (Kukhta and Bryce 2021), environmental purification (Xie et al. 2020; Wang et al. 2019), biomaterials (Zhou et al. 2020), solar energy conversion (Lee et al. 2017), sensors (Pięk et al. 2018), and in the field of medicine (Alam et al. 2018). These materials can combine very interesting optical (absorption, emission), electronic (insulating, semiconductor, metallic, or superconducting), and mechanical properties in the form of a single molecule, self-assembling single layers, or thin crystalline or amorphous films. The manufacture of thin-film has attracted considerable attention in the world in recent years due to its uses in different applications for different fields of research (Pan et al. 2019; Saadiah et al. 2019).

Organic dyes, in particular merocyanines dyes (Schembri et al. 2021), (Kulinich et al. 2018), and the metal–organic materials in the form of thin films, have been widely used in the last decades in various applications as energy transport materials, in particular for optoelectronic devices, dye

Responsible Editor: Philippe Garrigues

✉ Amina Laouid
laouidamina9@gmail.com

[1] Institute of Physics, Faculty of Physics, Astronomy and Informatics, Nicolaus Copernicus University in Toruń, Grudziadzka 5, PL 87-100 Torun, Poland

[2] National School of Applied Sciences, Engineering Science for Energy Laboratory, Chouaib Doukkali University of El Jadida, El Jadida, Morocco

[3] Centrer for Modern Interdisciplinary Technologies, Nicolaus Copernicus University in Toruń, Wilenska 4, PL 87-100 Torun, Poland

[4] LPHIA, SFR MATRIX, University of Angers, Physics Department, 2 Bd Lavoisier, 49045 ANGERS cedex 2, France

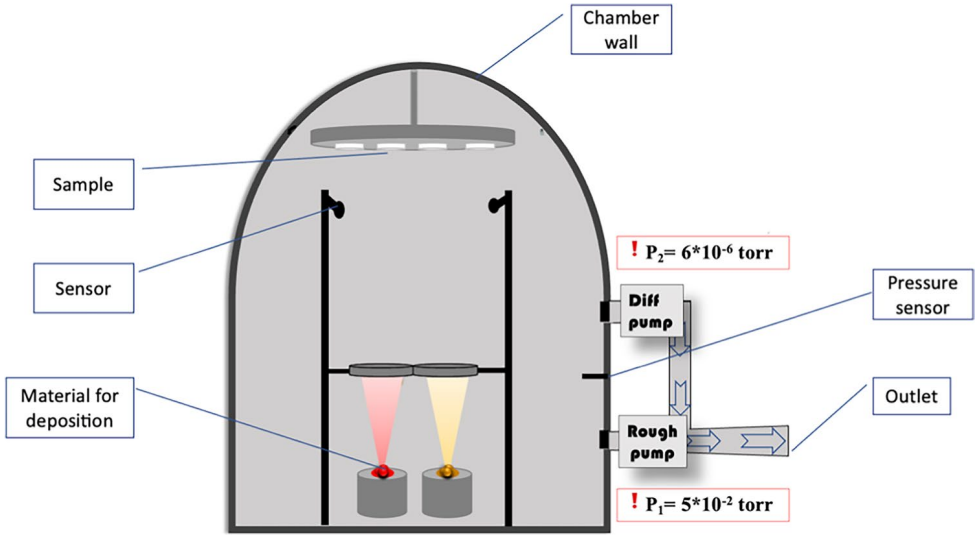


Fig. 1 Physical vapor deposition (PVD) apparatus

lasers, organic light-emitting diode (OLED), and solar cells, because of their interesting electrical and optical properties (Liess et al. 2019; Li et al. 2021; Pozin et al. 2021; Saeed et al. 2020; Gu and Zhang 2019; Ou et al. 2019).

4-(Dicyanomethylene)-2-methyl-6-(4-dimethylaminostyryl)-4H-pyran (DCM) is an organic coloring molecule that belongs to the class of merocyanines; it was first used by Eastman Kodak Company in 1997 as a doping material in the red color laser (Hong et al. 2021). This molecule contains a push–pull system which generally consists of an electron donor part and an electron acceptor part that are separated by a conjugated bridge, and this structure has attracted the attention of several research groups. It has shown great potential in its field due to its very interesting photophysical

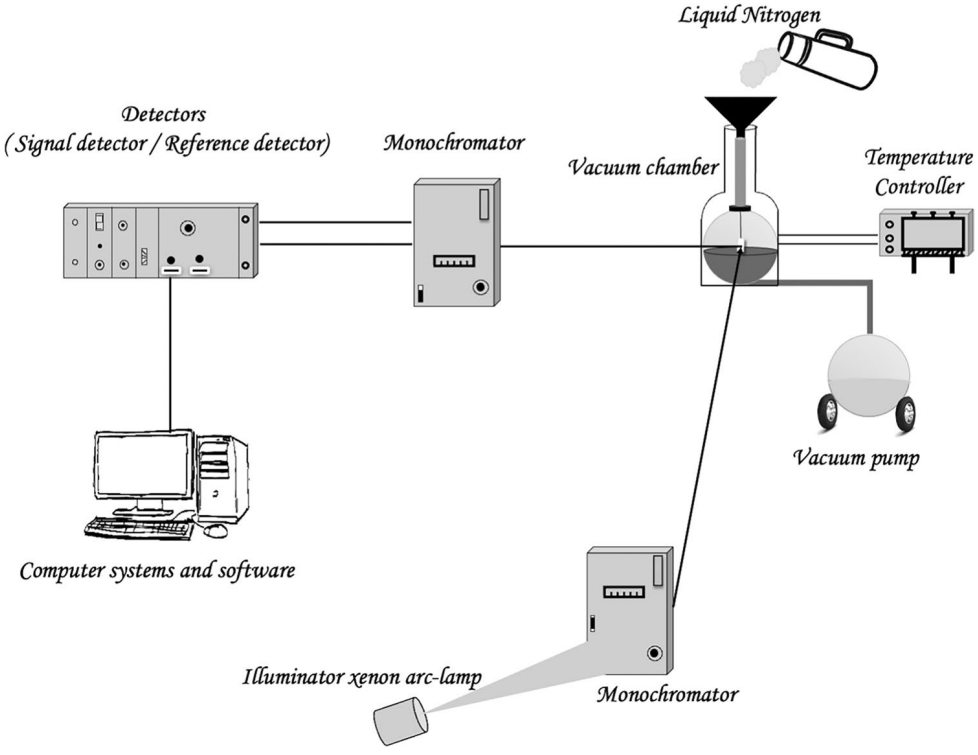


Fig. 2 Experimental setup for low-temperature photoluminescence measurements

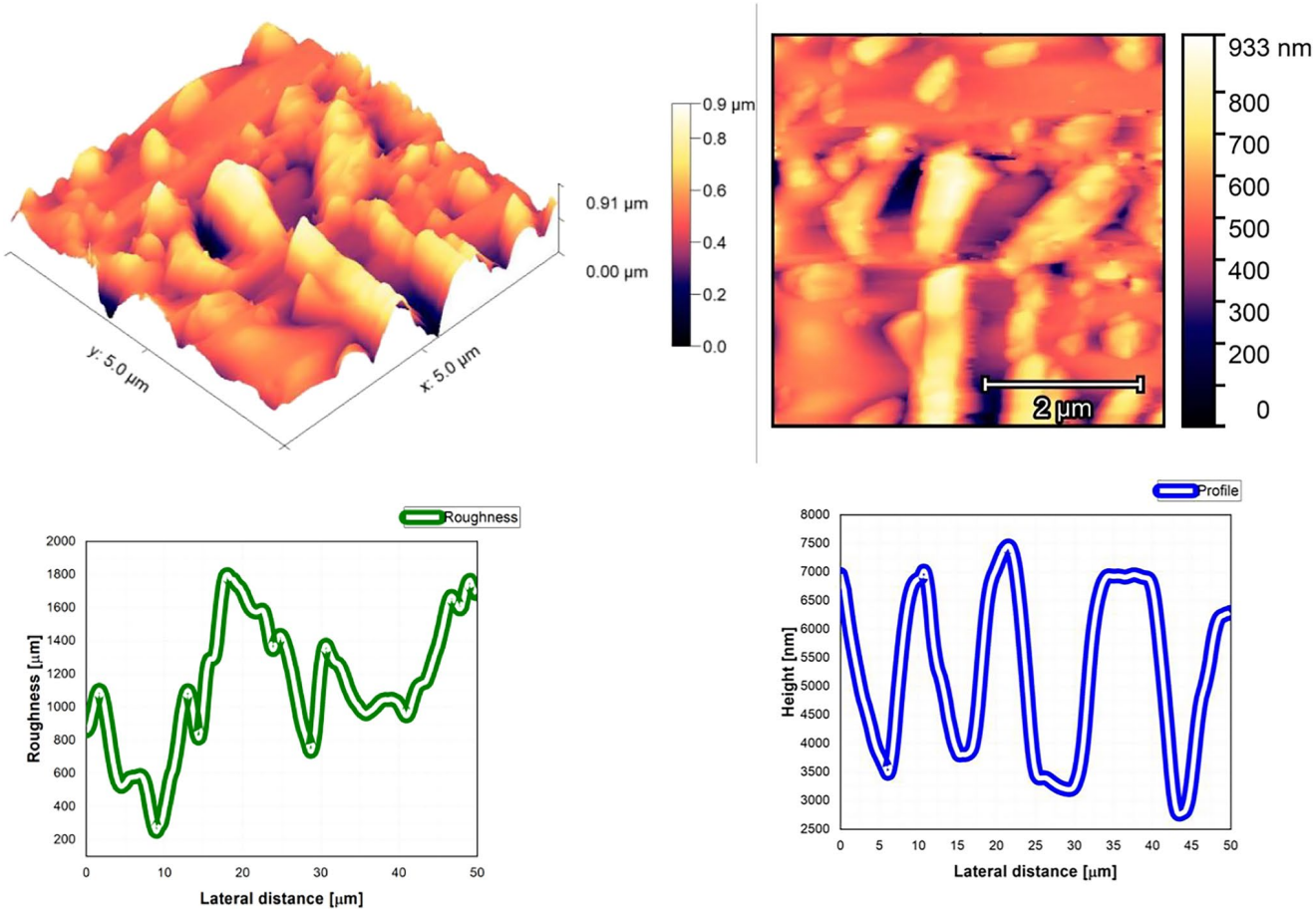


Fig. 3 AFM image, roughness and profile of DCM pure thin film (5 µm × 5 µm)

properties like its high fluorescence quantum efficiency, its absorption, and emission spectra, and also it has shown a large Stokes shift (Laouid et al. 2022). Therefore, it received great interest, which made it a basic material for several applications such as luminescent solar concentrators, photovoltaic, inorganic light-emitting diodes, and NLO applications (Popczyk et al. 2019; Waszkowska et al. 2020). This molecule contains a push–pull system which generally consists of a donor and an acceptor part of electrons (Noirbent et al. 2021). It has shown great potential in its field because of its very interesting photophysical properties (Weishäupl et al. 2021).

Studies on metal–organic materials, particularly metal–organic materials based on 8-hydroxyquinoline, remain a subject of interest due to their interesting and unique properties known for their fluorescence strength and significant non-linear optical properties (Kutluay 2021; Chen et al. 2022; About et al. 2021). Among these hydroxyquinoline compounds, we have a green luminescent material called bis(8-hydroxyquinoline) zinc (Znq_2). It is a semiconductor material that has attracted great interest from several researches' teams because of its mechanical, electrical, thermal, and chemical properties (Saito et al. 2021; Shinde et al. 2018; Li et al. 2019; Lougdali et al. 2022). Znq_2 has shown in front of aluminum tris (8-hydroxyquinoline) (Alq_3), which is the leader in its field in terms of luminescence efficiency and high quantum efficiency at a low operating voltage (Shahedi et al. 2017). This makes it an attractive material in various applications, such as medicine, photovoltaics, photonics, optoelectronics, and especially for OLED applications (Yuan et al. 2021; Shahedi et al. 2021).

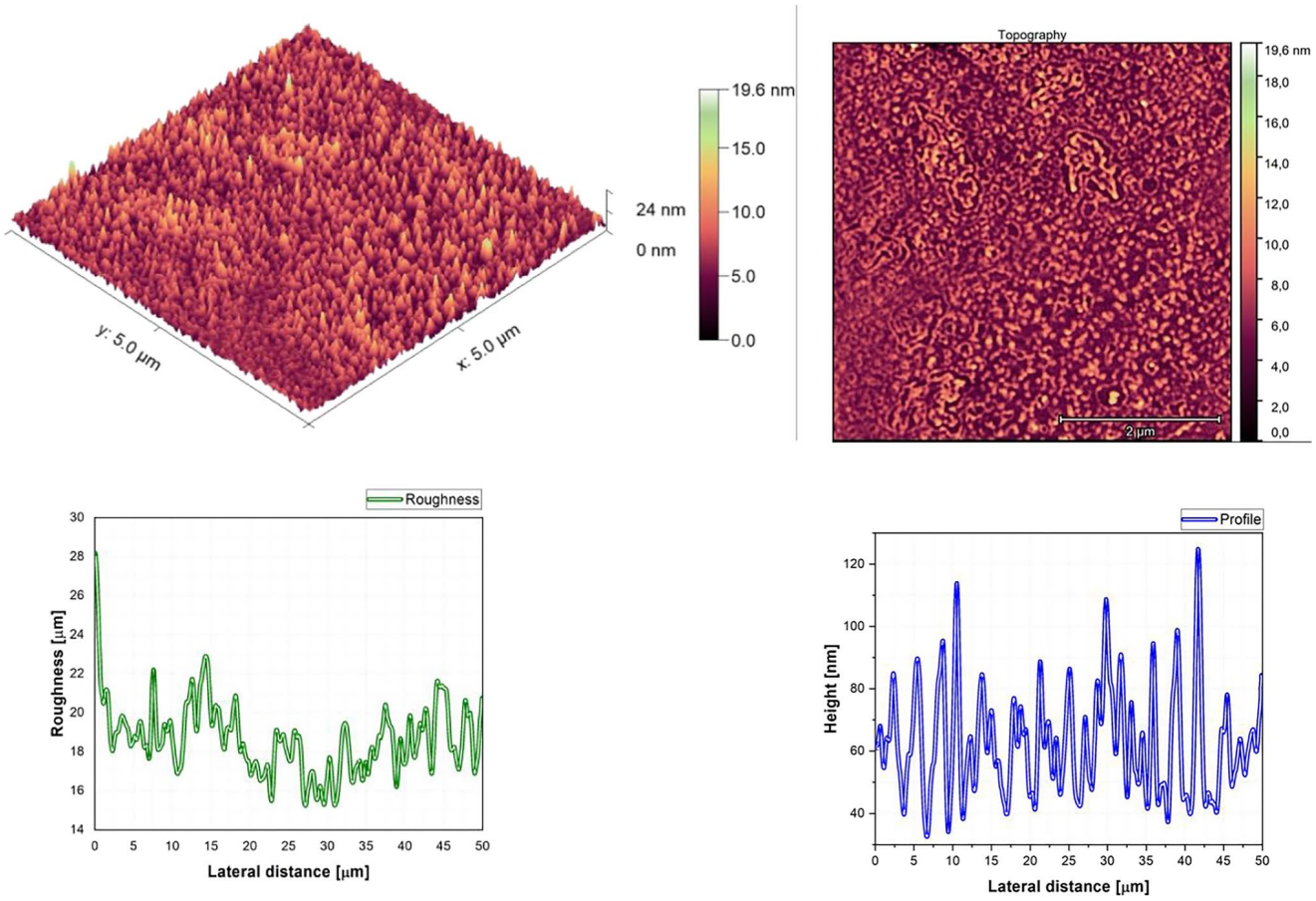


Fig. 4 AFM image, roughness and profile of Znq_2 pure thin film (5 µm × 5 µm)

On the other part, photoluminescence is a field that has been expanding and refining since the 1970s (Gilliland 1997). Photoluminescence spectroscopy is a powerful non-destructive optical technique, which allows to characterize semiconductor materials and also insulating materials (Yu and McCluskey 2021). Because of its good resolution, high precision, and high sensitivity, it has become an important technique in the study and engineering of materials. Time-resolved photoluminescence (TRPL) is a technique adapted to study the quick electronic deactivation processes that lead to the emission of photons in many types of materials such as metal–organic complexes and dyes. This fluorescence lifetime can be influenced by several parameters such as the molecular environment as well as by interactions with other molecules. This technique makes it possible to measure life in real time.

The main objective of this work is to manufacture organic thin films that are both environmentally friendly and represent a suitable candidate for optoelectronic applications; for this purpose, thin films of the different compositions of DCM and Znq_2 were developed using the vacuum evaporation technique in order to take advantage of the properties presented by these two materials. This paper is centered on the study of the impact of doping and temperature on photoluminescence and decay time, and also studied the transitions made to its various samples. The photoluminescence results obtained showed that the mixture of these organic compounds (DCM and Znq_2) present a very good alternative to produce optoelectronic devices and more particularly a very good one to generate red color lasers of good quality and very low cost.

Environmental Science and Pollution Research (2023) 30:81647–81666

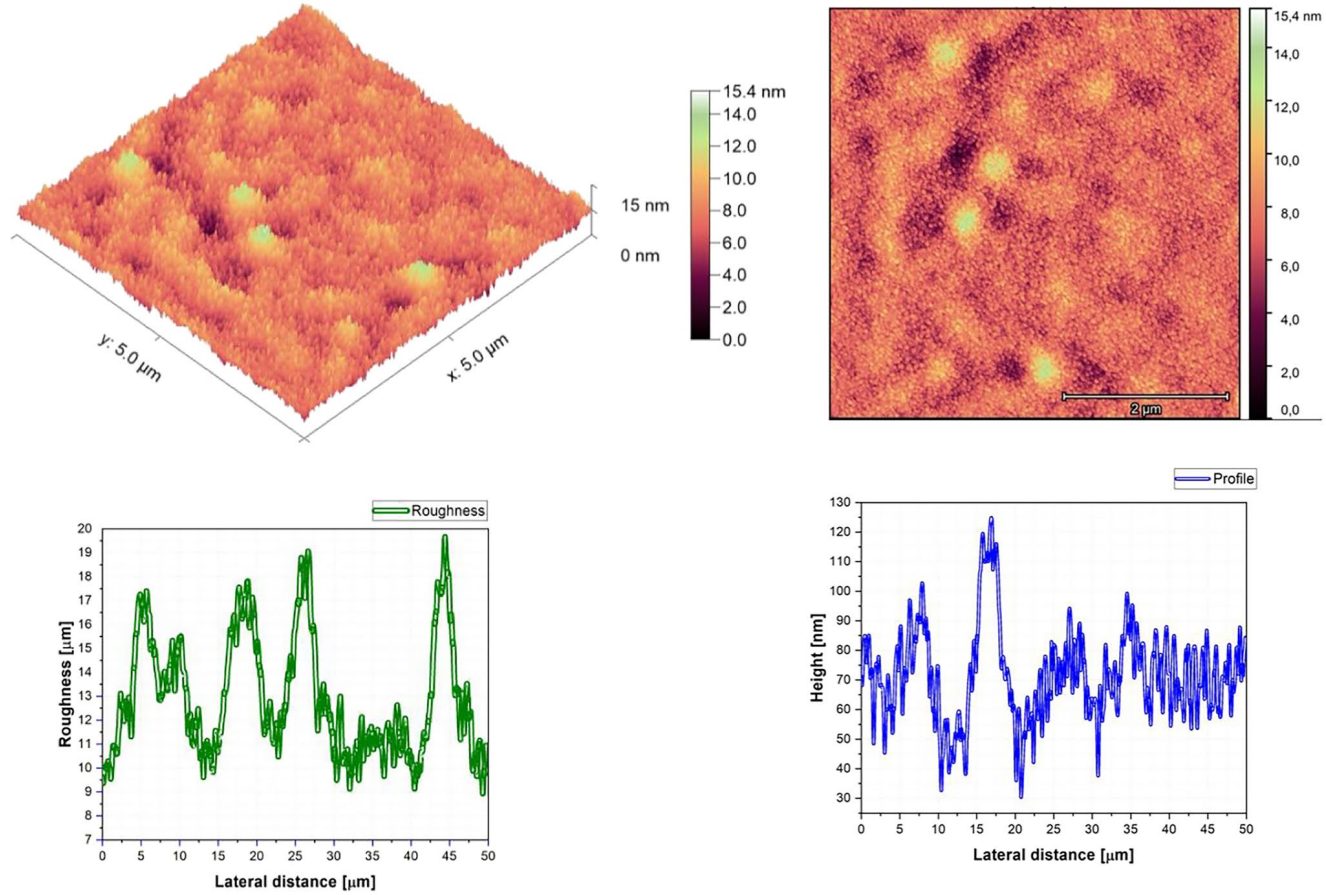


Fig. 5 AFM image, roughness and profile of 90%DCM-10%Znq_2 thin film (5 µm × 5 µm)

Experimental methods

Deposition technique of thin films

Since the glass surface quality has an impact on the properties of the thin films, cleaning is of considerable importance before starting the deposition. The cleaning method used consists of using an acetone bath with ultrasound for 15 min, then an ethanol bath, and finally, cleaning with isopropanol using flow synthesis.

The different samples were deposited on glass substrates using the vacuum evaporation technique under high vacuum 5×10^{-6}; the high vacuum is created by using two-pump diffusion pump and roughing pump is using the following system System-NANO 36™ (Kurt J. Lesker Company) (Popczyk et al. 2019).

Figure 1 shows the diagram of the co-deposition vacuum evaporation process. Powdered materials were purchased from Sigma-Aldrich and used without any purification. In order to obtain the optimal conditions for the deposition carried out in this experiment, the powders were placed separately in two aluminum oxide crucibles. Each crucible is placed in turn in a shielded tungsten crucible heater to control the temperature of the materials so that they have different deposition temperatures. The temperatures were controlled manually. The substrates are placed in a rotating holder. This study aims to deposit samples with different compositions and therefore the adjustment of the rates is a very important element; for this reason, the crucibles were covered until the rate control to ensure that the desired percentages were deposited, after adjusting all the parameters including density, Z-factor, and thickness of each element; checking the machine

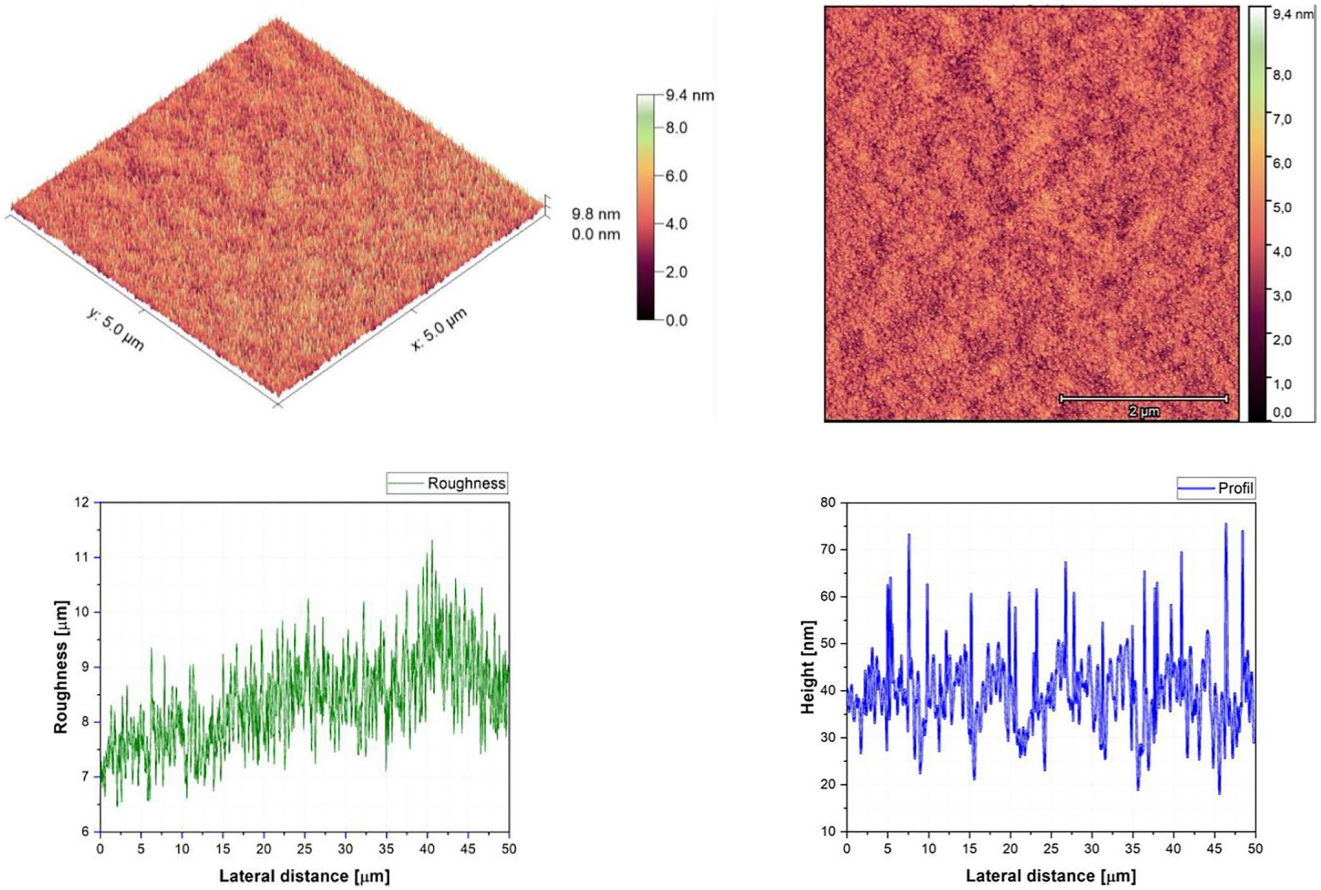


Fig. 6 AFM image, roughness and profile of 70%DCM-30%Znq_2 thin film (5 µm × 5 µm)

parameters, and also reaching the secondary vacuum which is another necessary parameter for the deposition as it provides a guarantee of film purity. The deposition process starts, and the powder starts to evaporate to form the thin film on the substrates. After obtaining the desired thickness (100 nm) with the help of the sensors, the deposition process stops automatically.

Characterization of thin films

In the present work, the atomic force microscopy technique (AFM) was used to examine the morphological properties of DCM co-doped Znq_2 thin films deposited on glass substrates. AFM imaging was studied in tapping mode, using the fiber-lite MI-150 equipment.

The photoluminescence of the thin layers grown on the glass substrate was measured by using FluoroMax-4 spectrofluorometer using FluorEssence software, and the source of excitation was a xenon lamp (Anoua et al. 2021; Zawadzka et al. 2019). This machine allows the measurement of excitation and emission as a function of the wavelength.

In order to study carefully the influence of the low temperature on the photoluminescence intensity of the samples, the measurements were carried out in the temperature interval of 77 to 300 K with a step of 25 K. The cooling was performed using liquid nitrogen. The

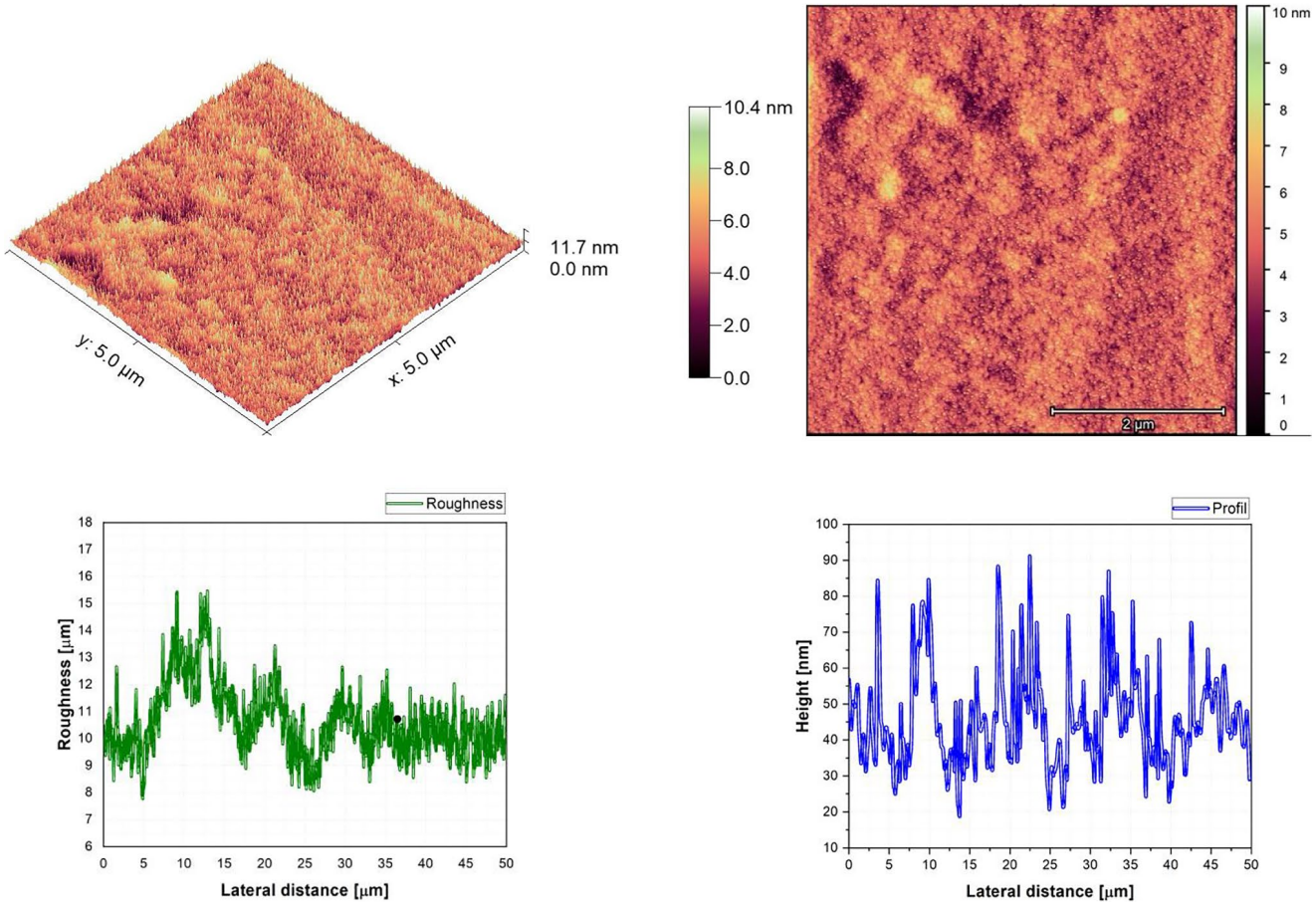


Fig. 7 AFM image, roughness and profile of 50%DCM-50%Znq_2 thin film (5 µm × 5 µm)

photoluminescence measurements were made inside a vacuum chamber under vacuum 10^{-3} torr as it is presented in Fig. 2. The substrate was attached to a temperature controller to adjust the temperature at each time.

Results and discussion

Morphological proprieties

The AFM pictures, roughness, and profile of each composition are presented in Fig. 3, Fig. 4, Fig. 5, Fig. 6, Fig. 7, Fig. 8, Fig. 9, and Fig. 10.

The AFM pictures demonstrate that doping influences the surface of the samples. For the images of the pure DCM sample, they showed a highly roughened (Average value ≈ 1.12 µm) surface with microscopic grains as shown in the film profile, while the sample of the pure Znq_2 showed a sponge structure with low thickness and manometric size granules are particularly noticeable. The other samples showed homogeneous morphology with a tendency to form nano spherical grains of a few nanometers in height as shown in the film's profiles. The samples of 90%DCM-10%Znq_2, 70%DCM-30%Znq_2, and 50%DCM-50%Znq_2 showed a flat surface with average roughness values respectively 12.9 nm, 9 nm, and 10 nm, while the samples of 20%DCM-80%Znq_2, 10%DCM-90%Znq_2, and 5%DCM-95%Znq_2 showed a sponge surface structure as in the case of pure Znq_2 with average roughness values respectively 7 nm, 10 nm, and 12 nm.

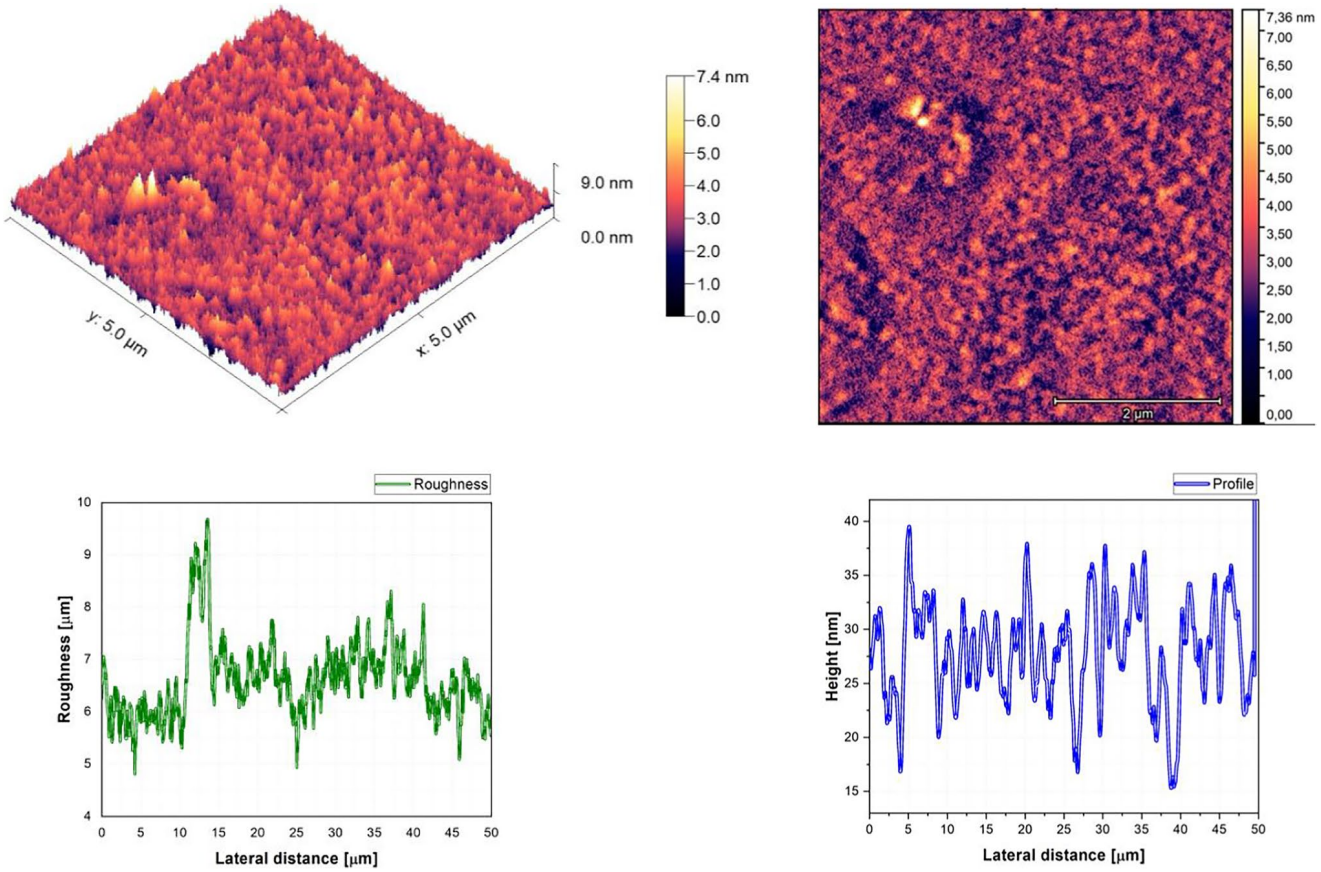


Fig. 8 AFM image, roughness and profile of 20%DCM-80%Znq_2 thin film (5 µm × 5 µm)

Photoluminescence at room temperature

For all samples except Znq_2, the emission spectrum measurements were studied from 500 to 850 nm, excited by 450 nm, while the excitation spectrum was measured in the range 300 to 600 nm at the maximum value of the emission intensity of about 645 nm. For thin films of Znq_2, its emission spectrum was studied from 450 to 700 nm, excited by 395 nm, while the excitation spectrum was measured in the range 200 to 500 nm at the maximum value of the emission intensity of about 536 nm.

The fluorescence changes of Znq_2 samples co-doped with DCM are shown in real images in Fig. 11.

The photoluminescence spectra of Znq_2-doped DCM thin films with different percentages are shown in Fig. 12.

The pure Znq_2 thin film showed strong luminescence in advance of the pure DCM thin film, while the highest luminescence intensity is that of the 5%DCM-95%Znq_2 sample. For the other samples, the intensity of photoluminescence is diminished compared to the pure Znq_2 thin film as the percentage of Znq_2 increases in the structure. For samples with a large percentage of Znq_2 (5%DCM-95%Znq_2, 10%DCM-20%Znq_2, 20%DCM-80%Znq_2), their PL spectra were shifted to orange (41 nm ± 5 nm) relative to the pure Znq_2 PL spectrum, and present three emission bands, as in the case of pure DCM. The first two bands had a low intensity at 490 nm and 504 nm respectively; however, the third most intense band is 614 nm. While in the samples with a large percentage of DCM (70%DCM-30%Znq_2, 90%DCM-10%Znq_2) their spectra

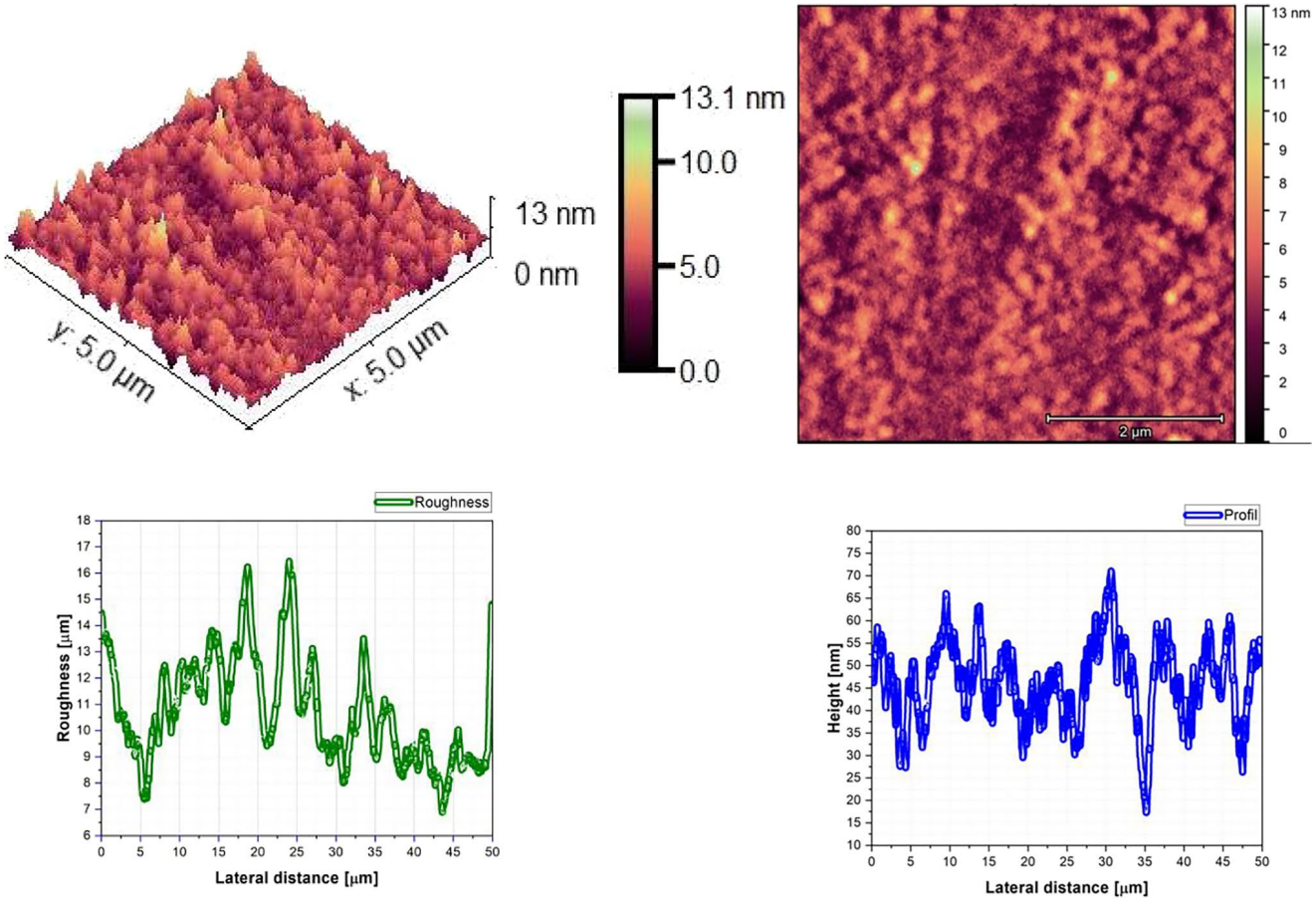


Fig. 9 AFM image, roughness and profile of 10%DCM-90%Znq_2 thin film (5 µm × 5 µm)

were shifted to red (with 116 nm), 50%DCM-50%Znq_2 sample has taken the character of pure DCM.

The samples with the different compositions of DCM and Znq_2 show peaks in the orange color emission region which is related to DCM; this result indicates that a complete energy transfer has occurred from Znq_2 to DCM due to the overlap between PL Znq_2 emission and DCM absorption Fig. 13. This is the same result found by Abedi et al. (2014) when they combined DCM with Alq_3.

As the observed PL spectra consist of a large band of visible luminescence, each spectrum was fitted with the Gaussian function in order to carefully study the transitions that occurred in the samples. The deconvoluted spectra involve several emission peaks, and each emission peak corresponds to a specific transition present in the particular sample; furthermore, the global spectrum is the sum of the corresponding Gaussian peaks. Figure 14 shows the deconvoluted PL spectra of all samples.

Through analysis of the fitted spectra, the pure DCM sample has presented five distinct characteristic peaks at or around 503 nm, 527 nm, 608 nm, 640 nm, and 692 nm. The pure Znq_2 thin film shows three distinct characteristic peaks at or around 515 nm, 546 nm, and 579 nm. Samples with a large percentage of DCM showed three emission bands around 601 ± 4 nm, 648 nm, and 695 nm ± 5 nm, while samples with a large percentage of Znq_2 have 4 emission bands around 490 nm, 506 ± 1 nm, 600 ± 4 nm, and 646 nm. Table 1 summarizes the results of the Gaussian fitting for emission spectra for all the samples at room temperature.

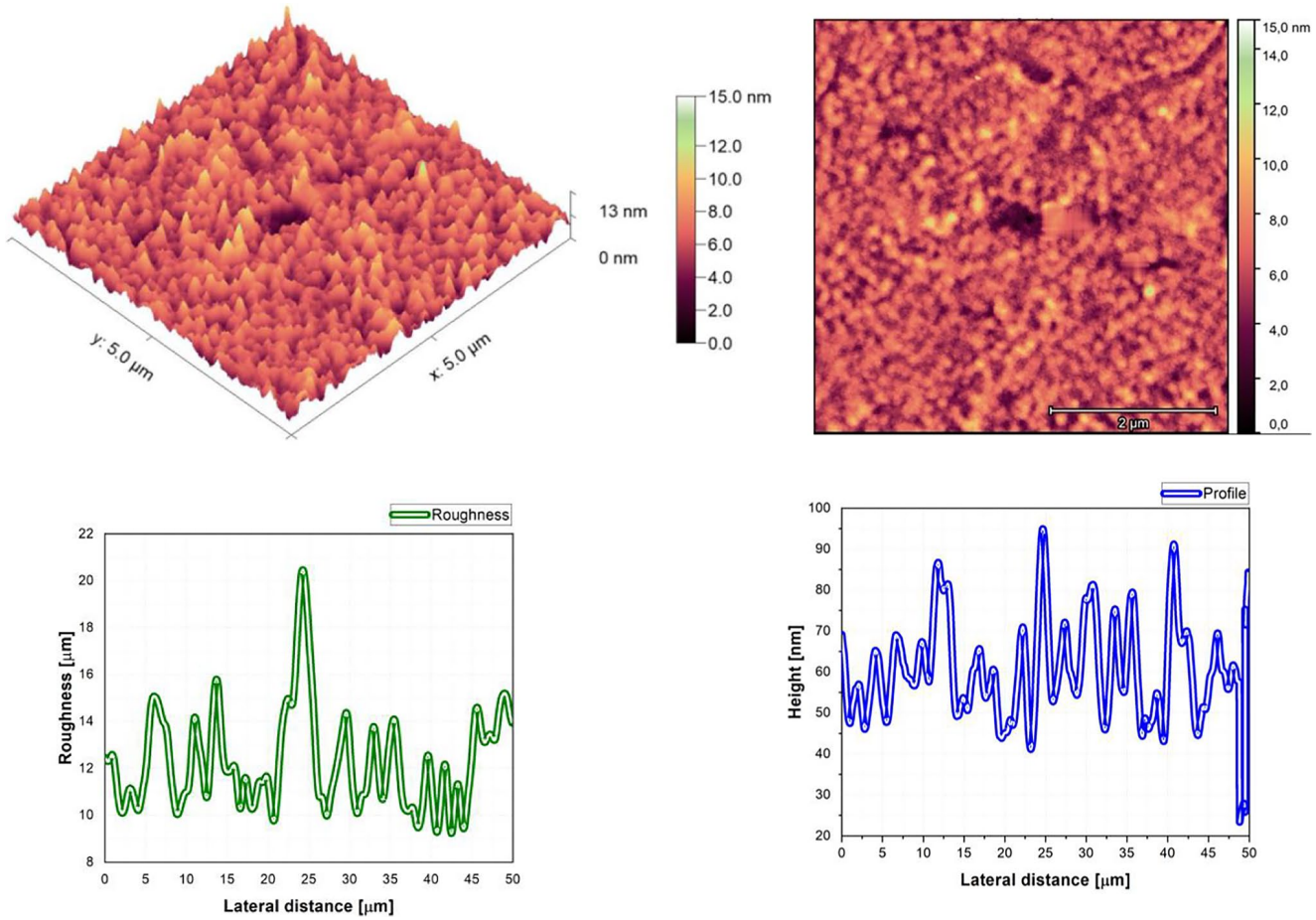


Fig. 10 AFM image, roughness and profile of 5%DCM- 95%Znq_2 thin film (5 µm × 5 µm)

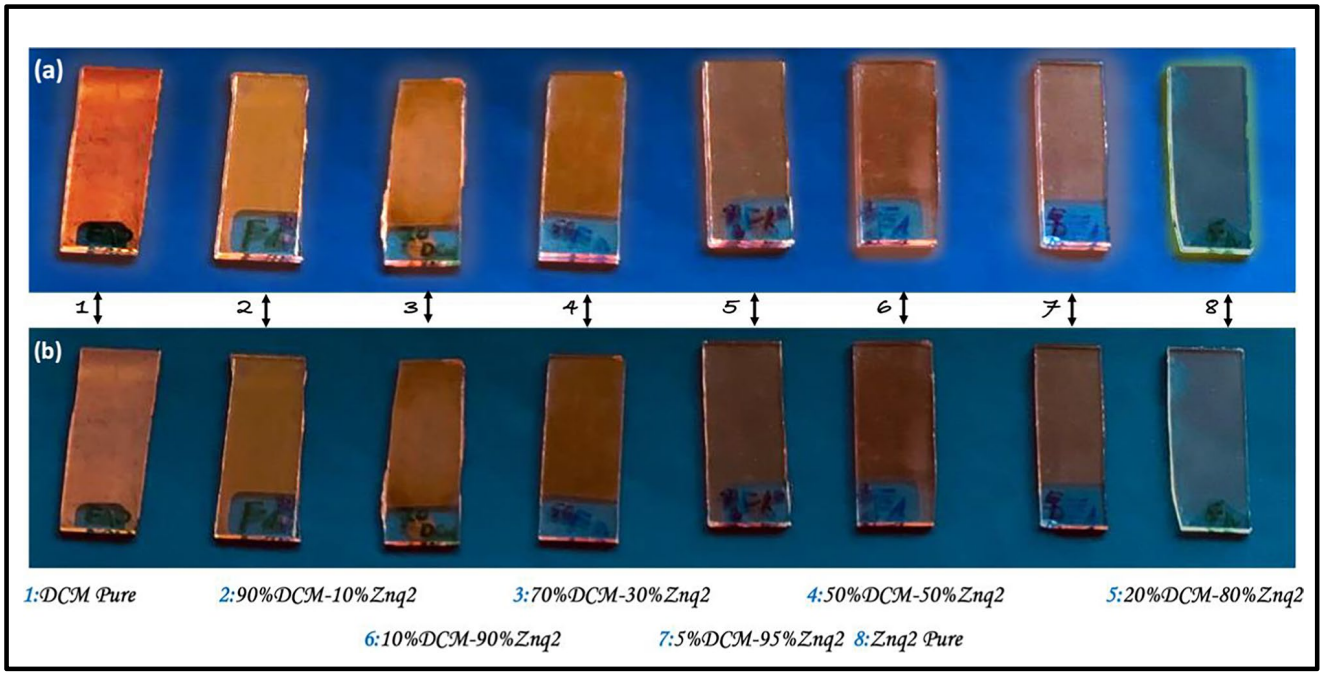
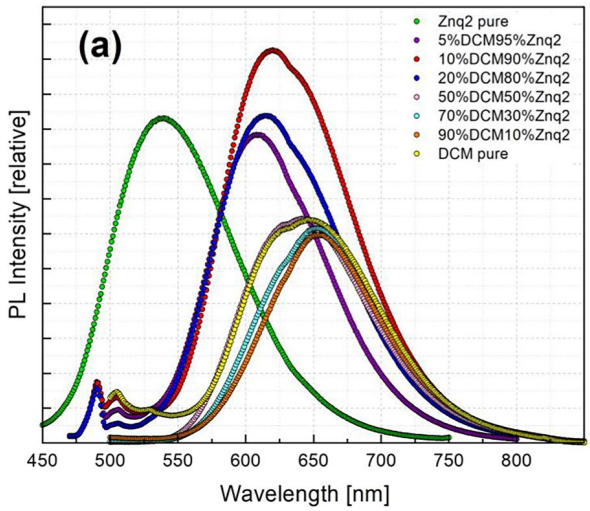


Fig. 11 The actual fluorescence changes of the Znq_2 Co-doped DCM samples. (**a**) The samples exposed to ultraviolet light and (**b**) the samples under normal conditions

Environmental Science and Pollution Research (2023) 30:81647–81666



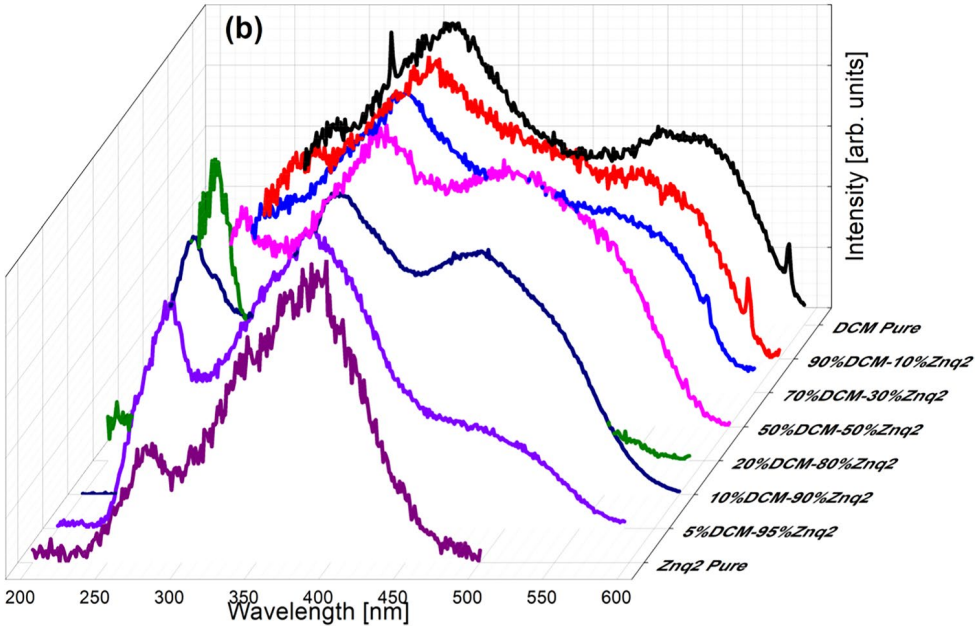


Fig. 12 **a** Emission, **b** excitation spectra at room temperature for all the samples

The emission bands of the pure DCM sample peaking at 503 nm, 527 nm, and 646 nm represent the characteristic bands, it can be attributed to the transition from HOMO → LUMO, HOMO-1 → LUMO, and HOMO → LUMO + 1. The other emission bands can be attributed to the excited and defect levels created in the film during deposition. The other thin films showed a dominance of red emission bands that are characteristic of pure DCM. They also showed new emission bands that depend on the percentage of Znq_2 in the structure.

The excitation spectra were also fitted by the Gaussian function, as shown in Fig. 15. The fitting of the excitations graphs allows to identify the transitions carried out inside

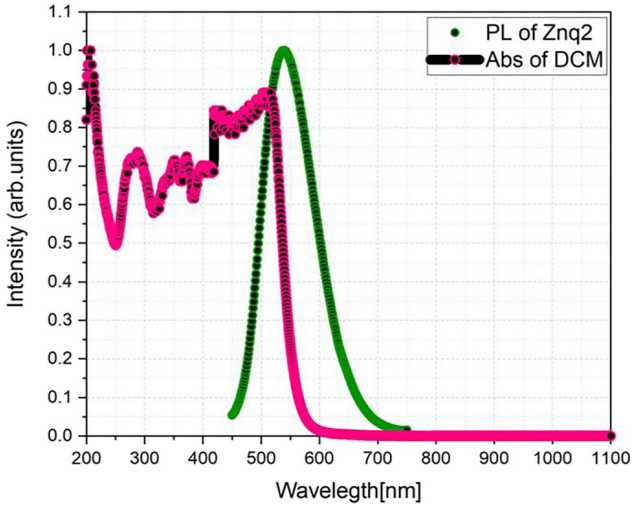


Fig. 13 Photoluminescence characteristic of Znq_2 and absorbance DCM

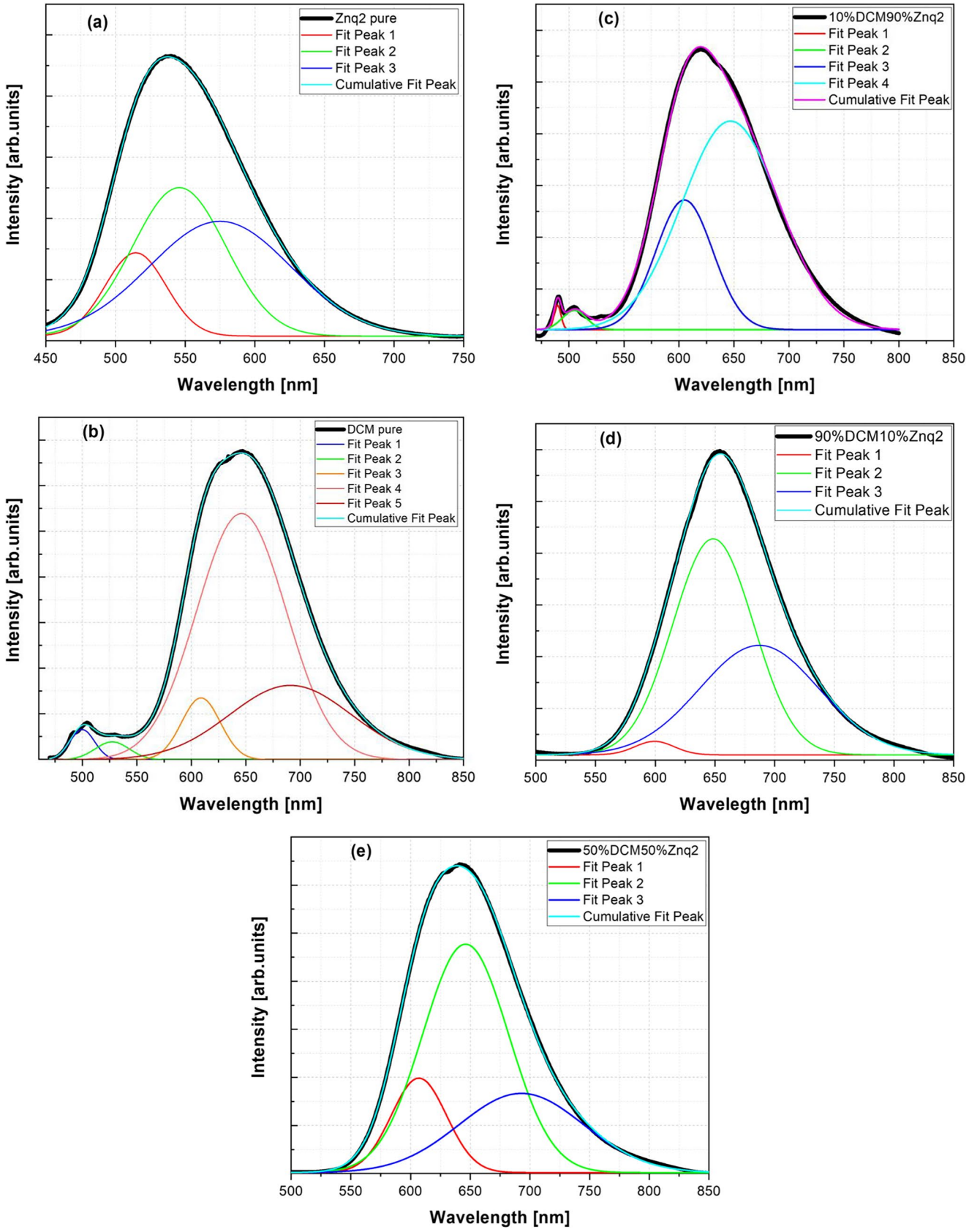


Fig. 14 Curves fitting for emissions spectra at room temperature of **a** Znq_2 pure, **b** DCM pure, **c** 10%DCM90%Znq_2, **d** 90%DCM10%Znq_2, **e** 50%DCM50%Znq_2

Table 1 Results of the Gaussian fitting for emission spectra for all the samples at room temperature. Xc in nm, height in CPS, and FWHM in nm

	Fit peak 1			Fit peak 2			Fit peak 3			Fit peak 4			Fit peak 5		
	Xc	Height	FWHM	Xc	Height	FWHM	Xc	Height	FWHM	Xc	Height	FWHM	Xc	Height	FWHM
DCM PURE	499	659535.14046	26.58845	527.33726	390638.97906	36.74496	608.82174	1.355355.86481	41.84463	640.03807	5396564.22015	96.8016	691.05649	1630946.77058	131.55236
Znq2	514.42161	2726313.05767	51.33698	545.69495	4854684.81121	78.70279	574.93722	3753124.97596	119.84472	–	–	–	–	–	–
5%DCM 95%Znq2	489.24916	1284663.27	7.98128	503.39739	769666.101	25.31	597.76339	4448217.32	63.59839	632.86541	5730050.93	105.46354	–	–	–
10%DCM 90%Znq2	489.6478	1386813.81	7.46383	504.92097	1224957.56	25.76946	604.85187	5429541.6	61.17927	646.85488	8508488.96	104.33478	–	–	–
20%DCM 80%Znq2	489.18938	1497170.35	9.08331	504.158687	603848.331	26.21	600.77929	5216751.56	66.99464	644.94822	6303056.03	106.33999	–	–	–
50%DCM 50%Znq2	–	–	–	–	–	–	606.92666	1990662.14	54.64879	646.07893	4787492.93	84.72181	692.82098	1679683.08	122.71296
70%DCM 30%Znq2	–	–	–	–	–	–	603.72772	582342.954	34.80091	648.48619	4892473.12	73.01478	695.92903	1800509.34	104.3869
90%DCM 10%Znq2	–	–	–	–	–	–	599.34227	261047.13556	38.55556	648.47274	4171336.11192	79.6351	687.07545	2114133.66569	117.65101

the thin film; more precisely, it gives a piece of information on the energy of gape of the thin films. Table 2 below summarizes the peaks' values found and their equivalent energies for all samples.

The pure Znq_2 film showed the presence of 4 peaks, while pure DCM film showed six peaks. Pure Znq_2 film has shown the transition that indicates their gape energy 2.9 eV (Monzon et al. 2011); this result is found by several research teams. The same for the pure DCM film has presented the transition of its gape energy 2.2 eV (Fujii et al. 1997; Qin et al. 2016).

The presence of the peak at 270 nm in all samples is well noted. The samples with different compositions, they presented from their turn six peaks. These peaks are also distinguished by the presence of the characteristic peaks of pure DCM and pure Znq_2 and also distinguished by the presence of new peaks which are the characteristic peaks of these samples. These results allowed us to confirm the presence of several transitions in the thin films. The fact that DCM belongs to the push–pull system which is both electron donor and acceptor, and Znq_2 has the character of an electron donor, the deposited films likely have a donor1-acceptor-donor2 chain form. And consequently, the structure has characteristic energy of pure DCM, of pure Znq_2, and more energies that are most likely related to the transition due to the interaction between A-D1 and the interaction between A-D2.

Temperature effect

The photoluminescence at low temperatures of thin films grown on a glass substrate with different compositions was also studied. Figure 16 shows the photoluminescence of all samples at low temperatures.

The 5%DCM-95%Znq_2, 10%DCM-90%Znq_2, and 20%DCM-80%Znq_2 samples showed a decrease in photoluminescence ranging from 77 to 175 k, then they increased sharply 810^3 CPS, 5 10^3 CPS, and 4 10^4 CPS respectively in the temperature range 200 to 275 K to reach the maximum, then it decreases while keeping the same position: 605 nm for 5%DCM-95%Znq_2, 600 nm for 10%DCM-90%Znq_2, and 612 nm for 20%DCM-80%Znq_2. While for the other samples, the most intense peak is obtained with the lowest temperature (77 k) and as the temperature increases the intensity of the peaks decreases; this decrease is accompanied by a change in the position of the peak maximum (1 nm for each 25 K).

The intensity of the photoluminescence of the elaborated samples is much higher at low temperatures; this dependence on the temperature can be explained by the non-radiative

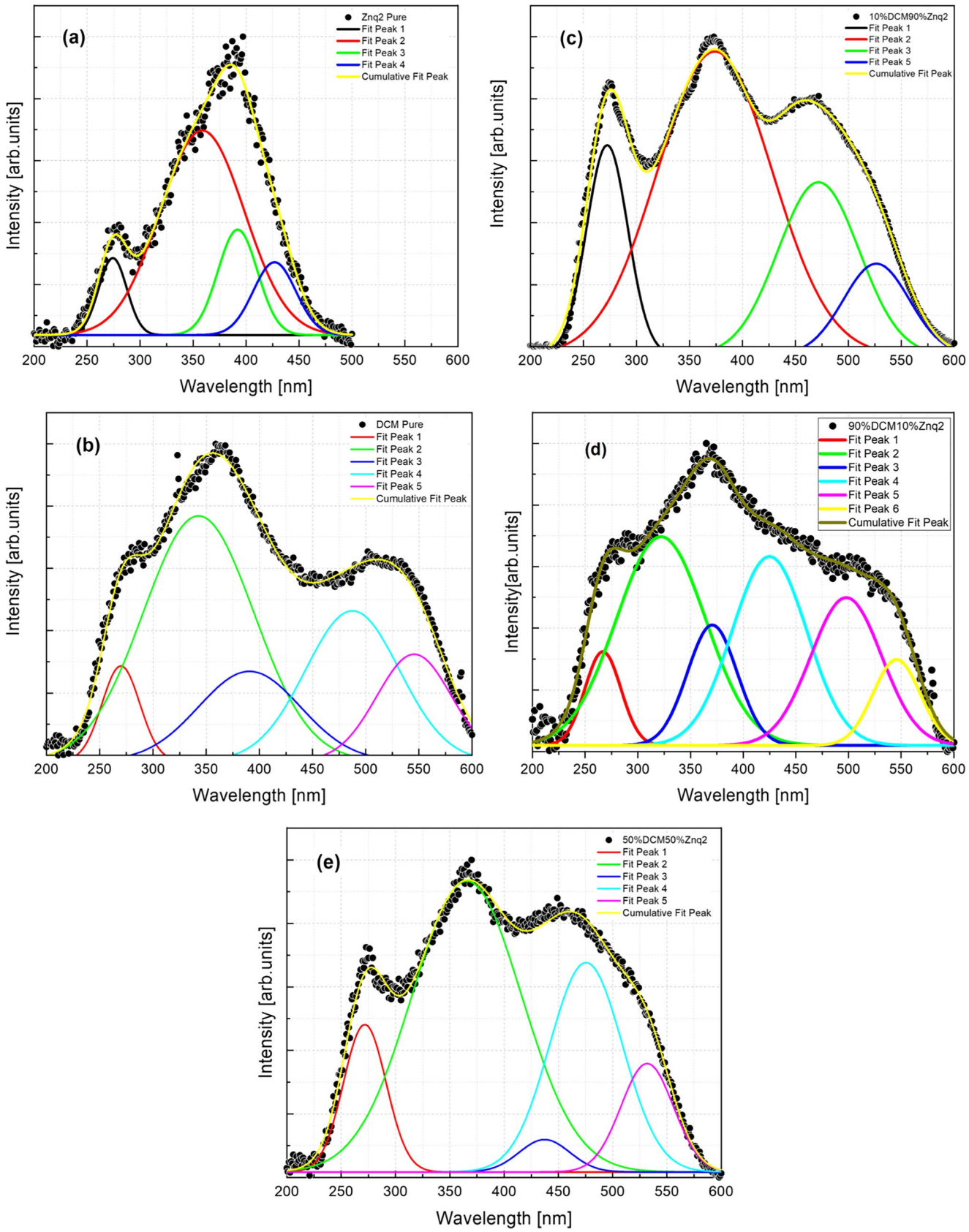


Fig. 15 Curves fitting for excitations spectra at room temperature of **a** Znq_2 pure, **b** DCM pure, **c** 10%DCM90%Znq_2, **d** 90%DCM10%Znq_2, **e** 50%DCM50%Znq_2

Table 2 Results of the Gaussian fitting for excitations spectra for all the samples at room temperature: peak in nm, Eg in eV

	Peak 1	E	Peak 2	E	Peak 3	E	Peak 4	E	Peak 5	E	Peak 6	E
DCM pure	269	4.6	319	3.8	366	3.38	408	3.03	509	2.43	550	2.25
Znq2 pure	270	4.59	356	3.5	392	3.16	427	2.9	–		–	
90%DCM10%Znq$_2$	269	4.6	319	3.8	371	3.34	420	2.95	490	2.53	545	2.27
70%DCM30%Znq$_2$	269	4.6	316	3.5	369	3.36	405	3.06	487	2.54	548	2.26
50%DCM50%Znq$_2$	269	4.6	330	3.9	369	3.36	418	2.96	476	2.6	535	2.31
20%DCM80%Znq$_2$	270	4.59	322	3.8	369	3.36	409	3.03	456	2.7	525	2.36
10%DCM90%Znq$_2$	269	4.6	315	3.9	370	3.36	430	2.88	470	2.63	525	2.36
5%DCM95%Znq$_2$	270	4.59	318	3.8	369	3.35	409	3.03	465	2.66	525	2.36

recombination of the photoexcited carriers which becomes more effective when we increase the temperature. Table 3 combines the data for the photoluminescence measurement of all films.

The most intense photoluminescence is obtained by the pure Znq_2 sample at low temperature, while for all other samples the DCM character dominates.

Decay time

Time-resolved photoluminescence (TRPL) is a technique adapted to study the quick electronic deactivation processes that lead to the emission of photons in many types of materials such as metal–organic complexes and dyes. This fluorescence lifetime can be influenced by several parameters such as the molecular environment as well as by interactions with other molecules. This technique makes it possible to measure life in real time.

The lifetime decay of the samples was measured at room temperature (300 K) using the FluoroMax-4 spectrofluorometer, which is connected to the FluoroHub single-photon counting controller using a pulsed diode as the excitation source (Zawadzka et al. 2014). The choice of the diode is related to the excitation wavelength.

Figures 17 and 18 show the decay time curves of all studied samples at different compositions. These curves show a transition between the ground state and the excited state and therefore are the results of the interaction between the emitting residues and their excited state of the films.

The spectra of all the films studied showed a decay with a nature of two exponentials. To properly analyze the lifetime decay of the samples, all the curves obtained are fitted with the bi-exponential function described by the following equation:

$$Y = A_1 e^{\frac{t}{\tau_1}} + A_2 e^{\frac{t}{\tau_2}} \quad (1)$$

where A_1 and A_2 are constants, t is pulse time, and τ_1 and τ_2 are decay values.

All samples showed two decay time components one short and one long. The Znq_2 film showed a longer exciton lifetime than the other samples $\tau_{1Znq2} = 3.47$ ns and $\tau_{2Znq2} = 10.96$ ns, while the samples with different compositions showed a dominance of the pure DCM film character even in the samples with a high percentage of Znq_2 as is presented in Fig. 18. The obtained values of the slowest decay components for the other samples are $\tau_1 = 0.09$ ns, while the values obtained of the highest decay component are $\tau_2 = 2.27$ ns. The average sample lifetime was also calculated $\tau_{av} = 1.18$ ns; consequently, the emission is fluorescence.

In polar environments, the DCM undergoes an intramolecular charge transfer (Kumar Kanaparthi et al. 2021; Lee

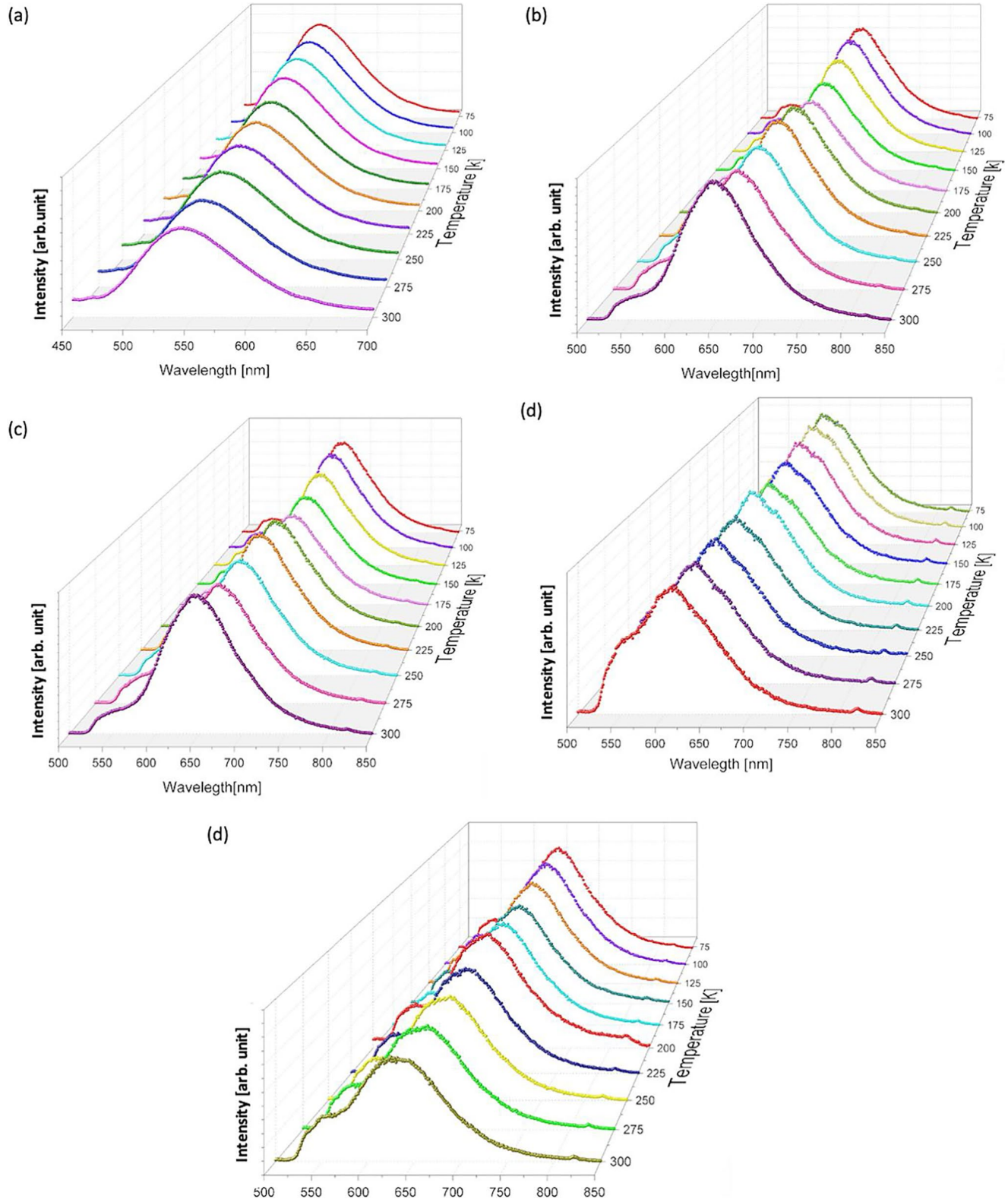


Fig. 16 Photoluminescence emission spectra at different temperatures for **a** Znq_2 pure, **b** DCM pure, **c** 90%DCM10%Znq_2, **d** 10%DCM90%Znq_2, **e** 50%DCM50%Znq_2

Table 3 Results of photoluminescence measurements at low temperatures

	DCM pure		Znq_2 Pure		5%DCM-95%Znq_2		10%DCM-90%Znq_2		20%DCM-80%Znq_2		50%DCM-50%Znq_2		70%DCM-30%Znq_2		90%DCM-10%Znq_2	
	PL (nm)	EW (CPS)	PL (nm)	EW (CPS)	PL (nm)	EW (CPS)	PL (nm)	EW (CPS)	PL (nm)	EW (CPS)	PL (nm)	EW (CPS)	PL (nm)	EW (CPS)	PL (nm)	EW (CPS)
77	661	$2.2\ 10^5$	537	$9.5\ 10^5$	605	$8\ 10^4$	613	$6.5\ 10^4$	602	$8.5\ 10^4$	648	$1\ 10^5$	659	$2.7\ 10^5$	662	$1.5\ 10^5$
100	660	$2.2\ 10^5$	537	$9\ 10^5$	604	$8.6\ 10^4$	613	$6.5\ 10^4$	602	$8.5\ 10^4$	647	$1\ 10^5$	659	$2.7\ 10^5$	662	$1.5\ 10^5$
125	659	$2.1\ 10^5$	537	$8.8\ 10^5$	604	$8.9\ 10^4$	613	$6.4\ 10^4$	602	$8.2\ 10^4$	645	$9.9\ 10^4$	659	$2.6\ 10^5$	661	$1.4\ 10^5$
150	658	$1.9\ 10^5$	537	$8.4\ 10^5$	604	$8.9\ 10^4$	613	$6.2\ 10^4$	602	$8\ 10^4$	644	$9\ 10^4$	657	$2.6\ 10^5$	658	$1.3\ 10^5$
175	657	$1.8\ 10^5$	539	$7.7\ 10^5$	604	$9.5\ 10^4$	613	$6.4\ 10^4$	602	$7.7\ 10^4$	643	$8.9\ 10^4$	655	$2.5\ 10^5$	656	$1.2\ 10^5$
200	656	$1.8\ 10^5$	540	$7.6\ 10^5$	604	$1\ 10^5$	613	$6.6\ 10^4$	602	$1.1\ 10^5$	641	$9.8\ 10^4$	652	$2.7\ 10^5$	660	$1.4\ 10^5$
225	655	$1.7\ 10^5$	540	$7.3\ 10^5$	604	$1\ 10^5$	613	$6.6\ 10^4$	602	$1.2\ 10^5$	640	$8.6\ 10^4$	652	$2.6\ 10^5$	654	$1.5\ 10^5$
250	652	$1.5\ 10^5$	540	$7\ 10^5$	604	$1\ 10^5$	613	$6.6\ 10^4$	602	$1.3\ 10^5$	639	$8.2\ 10^4$	650	$2.6\ 10^5$	653	$1.5\ 10^5$
275	649	$1.4\ 10^5$	540	$6.6\ 10^5$	604	$1\ 10^5$	613	$6.2\ 10^4$	602	$1.3\ 10^5$	638	$7.8\ 10^4$	649	$2.4\ 10^5$	651	$1.5\ 10^5$
300	648	$1.4\ 10^5$	540	$6.4\ 10^5$	604	$1\ 10^5$	613	$6.2\ 10^4$	595	$8.9\ 10^4$	630	$7.5\ 10^4$	644	$2.1\ 10^5$	644	$1.6\ 10^5$

et al. 2018) but in the following study we work on thin films, and due to the rigid environment hindering the movement of the molecules it is impossible that this phenomenon will occur, and therefore it is very likely that there is a Forster resonance energy transfer phenomena which results in non-radiative energy transfer from the donor fluorophore in the excited state to an acceptor molecule via a Coulomb interaction (Sasaki et al. 2016); this hypothesis can be reinforced by the spectral overlap of the emission spectra of the donor and the absorption spectra of the acceptor. The presence of the two decay times in pure DCM can be explained by two different physical processes illustrated in the transitions that occur from the ground state to the excited state of the donor and the transition from the ground state to the excited state of the acceptor, while for pure Znq_2 samples, a study suggests that the presence of the two decomposition rates is made up of two distinct physical processes that take place during the transfer of energy from the ground state to a higher state or a central metal atom to a quinoline ligand (Painuly et al. 2020).

Conclusion

In summary, DCM and Znq_2, which are red and green luminescent materials, respectively, were deposited under a high vacuum as thin films on glass substrates by the vacuum evaporation method. The emission spectra data shows that a small percentage of DCM inside Znq_2 can increase the photoluminescence intensity of the film; it also showed that a shift in the peak positions of the samples was also carried out which confirm that a complete energy transfer occurred from Znq_2 to DCM due to the overlap between the PL emission of Znq_2 and the absorption of DCM. Excitation spectra data showed in its turns the presence of more than one transition in the different samples. Low-temperature photoluminescence spectra showed that the photoluminescence intensity of the processed samples is much higher at low temperature; this temperature dependence can be explained by the non-radiative recombination of the photoexcited carriers which becomes more efficient when the temperature is increased. The time-resolved photoluminescence (TRPL) technique showed the presence of a single decay time in pure Znq_2 and two decay times for the other samples. The results obtained show that the combinations of these two materials are a good choice for optoelectronic applications.

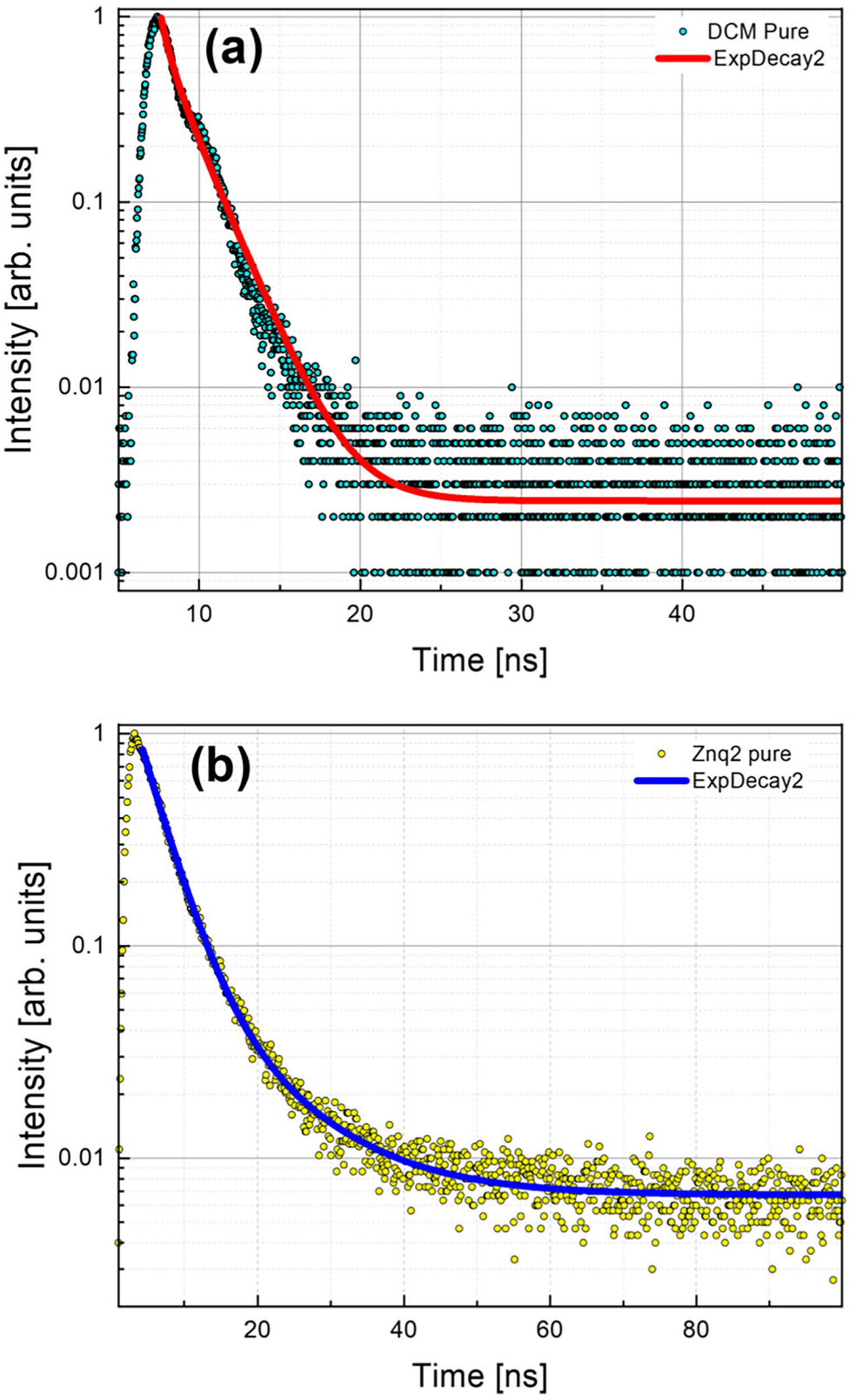


Fig. 17 Decay time curves **a** DCM pure and **b** Znq_2 pure at the maximum of luminescence wavelength at room temperatures of the measurements

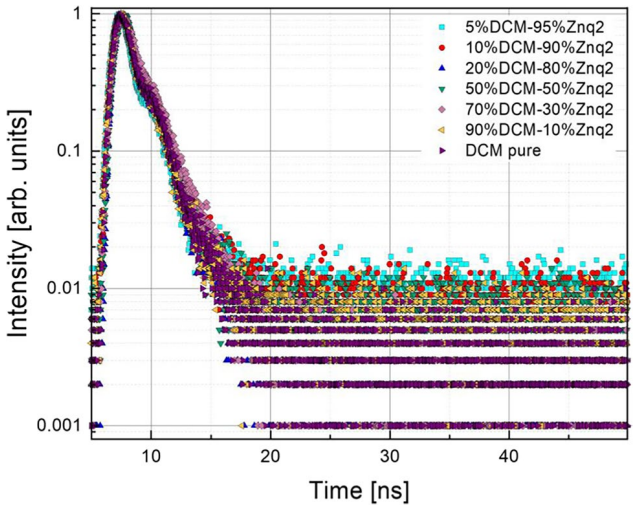


Fig. 18 Decay time curves for all the samples at the maximum of luminescence wavelength at room temperatures of the measurements

Author contribution A. Laouid: writing—original draft; formal analysis; experimental investigation; data curation.
A. Alaoui Belghiti: review and editing, formal analysis, supervision.
K. Wisniewski: review and editing, formal analysis, supervision.
A. Hajjaji: review and editing, formal analysis, supervision.
B. Sahraoui: methodology, visualization.
A. Zawadzka: experimental investigation, resources, methodology, supervision, funding acquisition.
All authors read and approved the final manuscript.

Funding This research has been financed from the funds of the Polish National Science Centre (grant no. 2017/25/B/ST7/02124). The films used in this paper were obtained using Interdisciplinary Centre for Modern Technologies facilities, NCU, Torun, Poland.

Availability of data and materials All data generated or analyzed during this study are included in this published article.

Declarations

Ethics approval Not applicable.

Consent to participate Not applicable.

Consent for publication Not applicable.

Competing interests The authors declare no competing interests.

Open Access This article is licensed under a Creative Commons Attribution 4.0 International License, which permits use, sharing, adaptation, distribution and reproduction in any medium or format, as long as you give appropriate credit to the original author(s) and the source, provide a link to the Creative Commons licence, and indicate if changes were made. The images or other third party material in this article are included in the article's Creative Commons licence, unless indicated otherwise in a credit line to the material. If material is not included in the article's Creative Commons licence and your intended use is not permitted by statutory regulation or exceeds the permitted use, you will need to obtain permission directly from the copyright holder. To view a copy of this licence, visit http://creativecommons.org/licenses/by/4.0/.

References

Abedi Z, Janghouri M, Mohajerani E et al (2014) Study of various evaporation rates of the mixture of Alq3: DCM in a single furnace crucible. J Lumin 147:9–14. https://doi.org/10.1016/j.jlumin.2013.10.020

About H, El Faydy M, Benhiba F et al (2021) Experimental and empirical assessment of two new 8-hydroxyquinoline analogs as effective corrosion inhibitor for C22E steel in 1 M HCl. J Mol Liq 325:114644. https://doi.org/10.1016/j.molliq.2020.114644

Alam AU, Qin Y, Nambiar S et al (2018) Polymers and organic materials-based pH sensors for healthcare applications. Prog Mater Sci 96:174–216. https://doi.org/10.1016/j.pmatsci.2018.03.008

Anoua R, Lifi H, Touhtouh S et al (2021) Optical and morphological properties of Curcuma longa dye for dye-sensitized solar cells. Environ Sci Pollut Res. https://doi.org/10.1007/s11356-021-14551-9

Chen Y, Wu L, Yao W et al (2022) A self-healing corrosion protection coating with graphene oxide carrying 8-hydroxyquinoline doped in layered double hydroxide on a micro-arc oxidation coating. Corros Sci 194:109941. https://doi.org/10.1016/j.corsci.2021.109941

Data P, Takeda Y (2019) Recent advancements in and the future of organic emitters: TADF- and RTP-active multifunctional organic materials. Chem Asian J 14:1613–1636. https://doi.org/10.1002/asia.201801791

Fujii N, Ohmori Y, Yoshino K (1997) An organic infrared electroluminescent diode utilizing a phthalocyanine film. IEEE Trans Electron Devices 44:1204–1207. https://doi.org/10.1109/16.605454

Gilliland GD (1997) Photoluminescence spectroscopy of crystalline semiconductors. Mater Sci Eng R Rep 18:99–399. https://doi.org/10.1016/S0927-796X(97)80003-4

Gu Z-G, Zhang J (2019) Epitaxial growth and applications of oriented metal–organic framework thin films. Coord Chem Rev 378:513–532. https://doi.org/10.1016/j.ccr.2017.09.028

Hong G, Gan X, Leonhardt C et al (2021) A brief history of OLEDs—emitter development and industry milestones. Adv Mater 33:2005630. https://doi.org/10.1002/adma.202005630

Kukhta NA, Bryce MR (2021) Dual emission in purely organic materials for optoelectronic applications. Mater Horiz 8:33–55. https://doi.org/10.1039/D0MH01316A

Kulinich AV, Ishchenko AA, Bulavko GV, Davidenko NA (2018) Effect of structure on the photovoltaic properties of merocyanine dyes in polymer films. Theor Exp Chem 54:178–185. https://doi.org/10.1007/s11237-018-9559-5

Kumar Kanaparthi R, Saha S, Singh M, Akhila M (2021) Photophysical properties of 4-(dicyanomethylene)-2-methyl-6-(4-dimethylaminostyryl)-4 *H* -pyran (DCM) and optical sensing applications. In: Photophysics, Photochemical and Substitution Reactions - Recent Advances. https://doi.org/10.5772/intechopen.93149

Kutluay S (2021) Excellent adsorptive performance of novel magnetic nano-adsorbent functionalized with 8-hydroxyquinoline-5-sulfonic acid for the removal of volatile organic compounds (BTX) vapors. Fuel 287:119691. https://doi.org/10.1016/j.fuel.2020.119691

Laouid A, Alaoui Belghiti A, Wisniewski K et al (2022) Structural and optical properties of DCM thin films prepared by PVD. Mater Today Proc. https://doi.org/10.1016/j.matpr.2022.03.244

Lee C-P, Li C-T, Ho K-C (2017) Use of organic materials in dye-sensitized solar cells. Mater Today 20:267–283. https://doi.org/10.1016/j.mattod.2017.01.012

Lee KJ, Lee YU, Fages F et al (2018) Blue-shifting intramolecular charge transfer emission by nonlocal effect of hyperbolic metamaterials. Nano Lett 18:1476–1482. https://doi.org/10.1021/acs.nanolett.7b05276

Li Y, Wu F, Han M et al (2021) Merocyanine with hole-transporting ability and efficient defect passivation effect for perovskite solar cells. ACS Energy Lett 6:869–876. https://doi.org/10.1021/acsenergylett.1c00124
Li Y, Zhong X, Xu Y et al (2019) Green synthesis and characterization of 8-hydroxyquinoline barium (BaQ2). Optik 180:151–158. https://doi.org/10.1016/j.ijleo.2018.11.090
Liess A, Arjona-Esteban A, Kudzus A et al (2019) Ultranarrow bandwidth organic photodiodes by exchange narrowing in merocyanine H- and J-aggregate excitonic systems. Adv Funct Mater 29:1805058. https://doi.org/10.1002/adfm.201805058
Lougdali M, Zazoui M, Abboud Y et al (2022) Linear and nonlinear optical properties of manganese bis-(8- hydroxyquinoline) thin films for optoelectronic devices: experimental and computational studies. J Mol Struct 1249:131558. https://doi.org/10.1016/j.molstruc.2021.131558
Monzon LMA, Burke F, Coey JMD (2011) Optical, magnetic, electrochemical, and electrical properties of 8-hydroxyquinoline-based complexes with Al3+, Cr3+, Mn2+, Co2+, Ni2+, Cu2+, and Zn2+. J Phys Chem C 115:9182–9192. https://doi.org/10.1021/jp201019c
Noirbent G, Pigot C, Bui T-T et al (2021) Synthesis, optical and electrochemical properties of a series of push-pull dyes based on the 2-(3-cyano-4,5,5-trimethylfuran-2(5H)-ylidene)malononitrile (TCF) acceptor. Dyes Pigments 184:108807. https://doi.org/10.1016/j.dyepig.2020.108807
Ou J, Xiang J, Liu J, Sun L (2019) Surface-supported metal–organic framework thin-film-derived transparent CoS1.097@N-doped carbon film as an efficient counter electrode for bifacial dye-sensitized solar cells. ACS Appl Mater Interfaces 11:14862–14870. https://doi.org/10.1021/acsami.8b21626
Pan L, Han Q, Dong Z et al (2019) Reactively sputtered WO3 thin films for the application in all thin film electrochromic devices. Electrochim Acta 328:135107. https://doi.org/10.1016/j.electacta.2019.135107
Painuly D, Singhal R, Kandwal P, Nagpure IM (2020) Structural, optical and decay properties of zinc(II) 8-hydroxyquinoline and its thin film. J Electron Mater 49:6096–6106. https://doi.org/10.1007/s11664-020-08255-y
Pięk M, Paczosa-Bator B, Smajdor J, Piech R (2018) Molecular organic materials intermediate layers modified with carbon black in potentiometric sensors for chloride determination. Electrochim Acta 283:1753–1762. https://doi.org/10.1016/j.electacta.2018.07.121
Popczyk A, Aamoum A, Migalska-Zalas A et al (2019) Selected organometallic compounds for third order nonlinear optical application. Nanomaterials 9:254. https://doi.org/10.3390/nano9020254
Pozin SI, Lypenko DA, Perelygina OM et al (2021) Polymer composite with J-aggregates of polymethine dye as a charge-transport layer of organic light-emitting diode. Inorg Mater Appl Res 12:94–100. https://doi.org/10.1134/S2075113321010354
Qin Y, Shi J, Gong X et al (2016) A luminescent inorganic/organic composite ultrathin film based on a 2D cascade FRET process and its potential VOC selective sensing properties. Adv Funct Mater 26:6752–6759. https://doi.org/10.1002/adfm.201601087
Saadiah MA, Zhang D, Nagao Y et al (2019) Reducing crystallinity on thin film based CMC/PVA hybrid polymer for application as a host in polymer electrolytes. J Non-Cryst Solids 511:201–211. https://doi.org/10.1016/j.jnoncrysol.2018.11.032
Saeed A, Alshahrie A, Salah N (2020) Fabrication of highly efficient organic light-emitting diode based on dysprosium-incorporated tris-(8-hydroxyquinoline)aluminum. J Mater Sci Mater Electron 31:22179–22189. https://doi.org/10.1007/s10854-020-04721-9
Saito N, Noda D, Shang Y et al (2021) Fluorescence and biological stabilization of phosphorus-functionalized mesoporous silica nanospheres modified with a bis(8-hydroxyquinoline) zinc complex. Mater Adv 2:6278–6282. https://doi.org/10.1039/D1MA00636C
Sasaki S, Drummen GPC, Konishi G (2016) Recent advances in twisted intramolecular charge transfer (TICT) fluorescence and related phenomena in materials chemistry. J Mater Chem C 4:2731–2743. https://doi.org/10.1039/C5TC03933A
Schembri T, Kim JH, Liess A et al (2021) Semitransparent layers of social self-sorting merocyanine dyes for ultranarrow bandwidth organic photodiodes. Adv Opt Mater 9:2100213. https://doi.org/10.1002/adom.202100213
Shahedi Z, Jafari MR, Zolanvari AA (2017) Synthesis of ZnQ2, CaQ2, and CdQ2 for application in OLED: optical, thermal, and electrical characterizations. J Mater Sci Mater Electron 28:7313–7319. https://doi.org/10.1007/s10854-017-6417-5
Shahedi Z, Zare H, Sediqy A (2021) Manufacturing of nanoflowers crystal of ZnQ2 by a co-precipitation process and their morphology-dependent luminescence properties. J Mater Sci Mater Electron 32:6843–6854. https://doi.org/10.1007/s10854-021-05389-5
Shinde P, Pandharipande S, Thejokalyani N, Dhoble SJ (2018) Exploration of photophysical properties of green light emitting bis(8-hydroxyquinoline) zinc (Znq2) metal chelate under various environments. Optik 162:151–160. https://doi.org/10.1016/j.ijleo.2018.02.075
Wang C, Kim J, Malgras V et al (2019) Metal–organic frameworks and their derived materials: emerging catalysts for a sulfate radicals-based advanced oxidation process in water purification. Small 15:1900744. https://doi.org/10.1002/smll.201900744
Waszkowska K, Cheret Y, Zawadzka A, Korcala A, El-Ghayoury A, Migalska-Zalas A, Sahraoui B (2020) Photoluminescence and nonlinear optical properties of triple stranded helicates based metallo-supramolecular architectures. Dyes Pigments 186:109036. https://doi.org/10.1016/j.dyepig.2020.109036
Weishäupl SJ, Mayer DC, Thyrhaug E et al (2021) A nitrophenyl-carbazole based push-pull linker as a building block for non-linear optical active coordination polymers: a structural and photophysical study. Dyes Pigments 186:109012. https://doi.org/10.1016/j.dyepig.2020.109012
Xie Z, Peng Y-P, Yu L et al (2020) Solar-inspired water purification based on emerging 2D materials: status and challenges. Sol RRL 4:1900400. https://doi.org/10.1002/solr.201900400
Yu Y, McCluskey MD (2021) Classification of semiconductors using photoluminescence spectroscopy and machine learning. Appl Spectrosc:000370282110316.https://doi.org/10.1177/00037028211031618
Yu M-H, Liu X-T, Space B et al (2021) Metal-organic materials with triazine-based ligands: from structures to properties and applications. Coord Chem Rev 427:213518. https://doi.org/10.1016/j.ccr.2020.213518
Yuan H, Zhang H, Yuan X et al (2021) Effect of electron and hole injection on spin polarization in bis-(8-hydroxyquinoline) zinc molecule. J Supercond Nov Magn. https://doi.org/10.1007/s10948-021-06077-5
Zawadzka A, Płóciennik P, Korcala A, Szroeder P (2019) Optical properties of chiral single-walled carbon nanotubes thin films. Opt Mater 96:109295. https://doi.org/10.1016/j.optmat.2019.109295
Zawadzka A, Płóciennik P, Strzelecki J (2014) Temperature-dependent luminescence dynamics for ZnO thin films. Opt Quantum Electron 46:87–101. https://doi.org/10.1007/s11082-013-9709-x
Zhou N, Liu T, Wen B et al (2020) Recent advances in the construction of flexible sensors for biomedical applications. Biotechnol J 15:2000094. https://doi.org/10.1002/biot.202000094

Publisher's note Springer Nature remains neutral with regard to jurisdictional claims in published maps and institutional affiliations.

Optical Materials 157 (2024) 116045

Contents lists available at ScienceDirect

Optical Materials

journal homepage: www.elsevier.com/locate/optmat

Research Article

Control of second-and third-order nonlinear optical properties of DCM and Znq_2 composites fabricated by the physical vapor co-deposition process

Amina Laouid [a,b,c,*], Houda El karout [d,e], Amine Alaoui Belghiti [b], Krzysztof Wisniewski [a,c], Przemysław Plociennik [c,g], Youssef El kouari [f], Bouchta Sahraoui [d], Abdelowahed Hajjaji [b], Anna Zawadzka [a,c]

[a] Institute of Physics, Faculty of Physics, Astronomy, and Informatics, Nicolaus Copernicus University in Toruń, Grudziadzka 5, PL 87-100 Torun, Poland
[b] Chouaib Doukkali University of El Jadida, National School of Applied Sciences, Engineering Science for Energy Lab, El Jadida, Morocco
[c] Centrer for Modern Interdisciplinary Technologies, Nicolaus Copernicus University in Toruń, Wilenska 4, PL 87-100, Torun, Poland
[d] Univ Angers, LPHIA, SFR MATRIX, F-49000, Angers, France
[e] Univ Angers, CNRS, MOLTECH-ANJOU, SFR MATRIX, F-49000, Angers, France
[f] Laboratory of Materials, Energy and Systems Control, Faculty of Sciences and Technology, Hassan II University of Casablanca, B.P 146, Mohammedia, Morocco
[g] Institute of Engineering and Technology, Faculty of Physics, Astronomy and Informatics, Nicolaus Copernicus University, Grudziadzka 5, PL 87-100, Torun, Poland

ARTICLE INFO

Keywords:
Thin films
Physical vapor deposition (PVD)
Nonlinear optic (NLO)
Third harmonic generation (THG)
Second harmonic generation (SHG)
DCM
Znq_2

ABSTRACT

In the present work, investigations on the second and third-order NLO properties of, 4-(dicyanomethylene)-2-methyl-6-(4-dimethylaminostyryl)-4H-pyran (DCM) reddye co-doped bis(8-hydroxyquinoline) Zinc (Znq_2) thin films with different concentrations were investigated. The samples have a thickness of 100 nm. They were prepared using the physical vapor deposition (PVD) method under a high vacuum. The morphological properties were studied by atomic force microscopy. The second-order nonlinear susceptibility $\chi^{(2)}$ after applying the corona poling technique was estimated using the comparative model of Lee, while the third-order nonlinear susceptibility $\chi^{(3)}$ was estimated using the comparative model of Kubodera and Kobayashi. The tested samples varied in terms of the concentration of DCM in the structure, which visibly influenced their nonlinear response. The pure DCM thin film showed a large value of the second and third-order nonlinear susceptibility, while pure Znq_2 had only the second harmonic response with a low value. In this study, we have demonstrated that doping with DCM, even with small concentrations, has also strongly enhanced the non-linearity of Znq_2. The obtained results show that such compositions can be a good alternative for optoelectronic applications.

1. Introduction

The research field of nonlinear optics (NLO) has received considerable interest over the years [1–4]. It concerns the processes that occur when a material medium is subjected to a light beam that is sufficiently intense to modify the response of the medium to the electromagnetic field [5,6]. Among these processes, we find the second harmonic generation (SHG), third harmonic generation (THG), and optical Kerr effect [1,7,8]. The most significant effect is that these processes can be "combined" or " divided" (sum and difference frequency generation), offering the possibility to manipulate the micro frequencies [9]. Several research teams are actively involved in developing the NLO field not only as a supplement to linear optics but also for its potential in other disciplines including high-resolution imaging, bioimaging, quantum optics, and optoelectronics [10–15]. As each medium has a different polarization intensity, the NLO behavior is strongly dependent on the type of material in the medium, which makes its application wide-ranging. Additionally, harmonic generation can be a reliable indicator of microstructural information or change due to its sensitivity to the crystal structural symmetry and nonlinear susceptibility is used to investigate the ability of materials to generate a nonlinear process [16].

NLO materials have attracted the attention of the scientific community due to their properties, which are useful in various applications such as imaging and optoelectronics [17–19]. Nevertheless, finding suitable NLO materials for the fabrication of electro-optic devices is not an easy task. Indeed, the high susceptibilities of these materials are

* Corresponding author. Institute of Physics, Faculty of Physics, Astronomy, and Informatics, Nicolaus Copernicus University in Toruń, Grudziadzka 5, PL 87-100, Torun, Poland.
E-mail address: laouidamina9@gmail.com (A. Laouid).

https://doi.org/10.1016/j.optmat.2024.116045
Received 18 January 2024; Received in revised form 27 August 2024; Accepted 1 September 2024
Available online 2 September 2024
0925-3467/© 2024 Elsevier B.V. All rights are reserved, including those for text and data mining, AI training, and similar technologies.

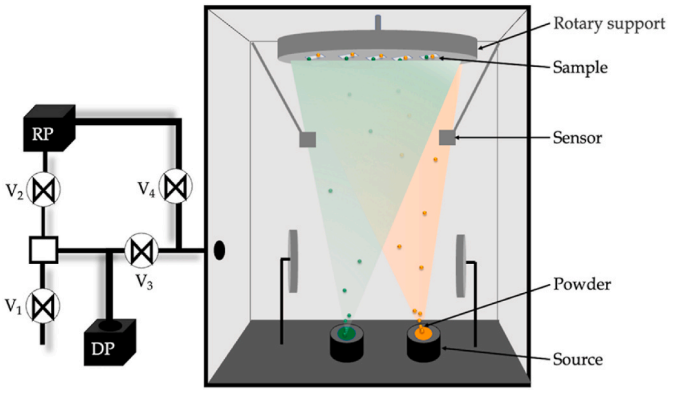


Fig. 1. Physical vapor co-deposition (PVD) apparatus: DP, diffusion pump; RP, rotary vacuum pump; V_1,V_2,V_3 and V_4 valves.

necessary for the development of electro-optical devices and all-optical data processing systems. Due to the electronic structure of materials with conjugated π-electron systems, the optical properties are often much more non-linear with a fast response compared to inorganic materials [20].

In particular, bis(8-hydroxyquinoline) Zinc (Znq_2) thin films have been studied for many years due to their potential in several fields, including optoelectronics, photovoltaics, and photonics [21–24]. Due to their unique intramolecular structure that allows them to exhibit great electron transfer properties and their ability to emit light in the visible range, both linear and nonlinear optical properties have been extensively studied [22,25,26]. Znq_2 is distinct from other compounds due to it significant potential as a third-order nonlinear material. This is mainly because of its ability to exhibit switchable nonlinearity, which arises from two key factors: (1) the multiple accessible electronic states of the central zinc atom, which can undergo transitions under external fields, and (2) the charge transfer interactions between the zinc atom and the surrounding 8-hydroxyquinoline ligands. These charge transfer processes, facilitated by the coordination environment of the zinc, enable reversible changes in the electronic distribution, thereby allowing for the modulation of nonlinear optical properties [27–29].

On the other hand, 4-(dicyanomethylene)-2-methyl-6-(4-dimethylaminostyryl)-4H-pyran (DCM), as a push-pull molecule containing electron-donating (D) and electron-accepting (A) groups connected by a π-conjugated bridging group (D-π-A system) are of particular interest [30–34]. This interest is due to their applications in optoelectronics, e.g., in organic light-emitting diodes, light-emitting sensors, and semiconductor lasers [35,36]. The important characteristics of this type of material are mainly related to the extended π-conjugated systems [37,38]. DCM belonging to the merocyanine family (red dye), exhibits very interesting photophysical properties such as tunable electronic absorption and fluorescence emission energies and high fluorescence quantum yields. However, the nonlinear optical responses of DCM as a thin film are still limited [39,40].

Motivated by the properties presented by the two materials, thin films with different compositions of DCM and Znq_2 have been prepared by vacuum evaporation technique. The morphological properties have been developed by using the atomic force microscopy technique. The nonlinear properties more precisely the second and third harmonic responses of these thin films with different compositions have been studied for the first time in this work. In particular, a comparative study is carried out on the different compositions of the thin films in order to study the influence of doping on the nonlinear properties. Pure DCM has shown a very good nonlinear response.

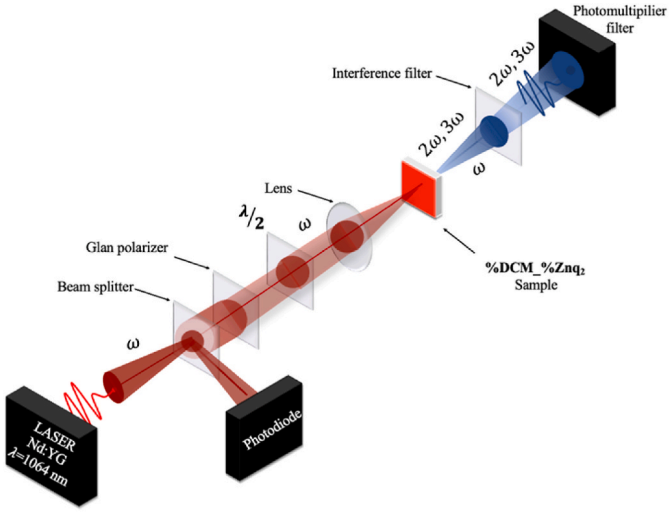


Fig. 2. Experimental set-up for SHG and THG measurements.

2. Experimental methods

2.1. Preparation of thin films

DCM and Znq_2 powders were purchased from Sigma-Aldrich and used as is without any further purification. Pure and DCM-doped Znq_2 thin films were prepared on a glass substrate by the physical vapor deposition (PVD) method.

The process of deposition was performed using a vacuum system called "thin film Deposition System - NANO 36™" (Kurt J. Lesker Company) [34–36,41,42]. The deposition is carried out inside the vacuum chamber, under a very high vacuum (1.3 $*10^{-5}$ torr) Fig. 1. The thickness of the deposited layer will depend on the evaporation rate, the geometry of the source, the substrate, the evaporation time, and the distance between the substrates and the source. The DCM and Znq_2 powders were positioned on two different crucibles and the distance between them and the glass substrates was equal to 20 cm. During the whole deposition process, the substrates were rotated at a speed of 20 rpm, while the film thicknesses and deposition rates were monitored by piezoelectric sensors. The deposition process automatically stopped when the desired thin film thickness was achieved. The thin film thickness was determined by the vacuum system using a piezoelectric detector.

2.2. Atomic force microscopy measurements

The morphological properties of the studied thin films were examined by the atomic force microscopy (AFM) technique in contact mode. The measurements were carried out at room temperature by using Nanosurf easy Scan 2 AFM XYCONTR cantilever microscope [30,43].

2.3. UV–visible measurements

A double-beam spectrophotometer (PerkinElmer Lambda 2 UV/VIS/NIR) was used to measure the transmission spectra of the deposited thin films at normal incidence in the spectral range 190–1100 nm [44].

2.4. NLO measurements

The second and third-order nonlinear optical effects were studied using second and third-harmonic generation techniques. The measurements were performed in the transmission scheme using the Maker rotating fringe technique with a quartz sample plate as reference material by rotating the sample from −60° to 60° on a rotating table [45,

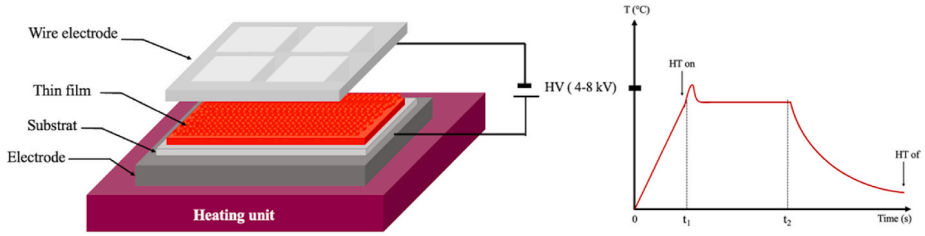


Fig. 3. Diagram of the experimental set-up used for corona poling.

46]. A pulsed Nd:YAG laser (PL2250, Ekspla) generating a wavelength of 1064 nm (pulse duration – 30 ps) was used as the light source, and the intensities of the generated harmonics as a function of the rotation angle were obtained. Second-order measurements were performed in a vertically (P) and horizontally (S) polarized fundamental beam. An interference filter was placed in alignment to cut the main wavelength of the generated residual harmonics Fig. 2.

2.5. The "Corona poling" technique

The Corona poling method is widely used, and it corresponds to the heat treatment under an electric field. It is used to orient the material to break the centrosymmetry for some mediums. The nonlinear medium must be non-centrosymmetric in order to optimize the efficiency of conversion of the fundamental wave to the harmonic. The orientation of the molecules allows a significant increase in the efficiency of the second harmonic generation process [47,48].

The experimental set-up allowing the orientation of the molecules is represented in Fig. 3.

The principle of this method is as follows: Firstly, the system is initially heated to the material's glass transition temperature (0 to t_1) which is the temperature range in which the material transitions from a hard and relatively brittle state into a viscous or rubbery state. This state change is crucial as it allows the molecules within the material to reorient themselves more freely under the influence of the applied electric field.

Once the material reaches thermal equilibrium at the glass transition temperature, a high voltage is applied between the wire electrode and the substrate electrode. The electric field generated by this voltage induces a preferential orientation of the molecular dipoles within the material. This alignment breaks the initial centrosymmetry, a necessary condition for second harmonic generation in nonlinear optical processes.

The high voltage is maintained while the material is held at the glass transition temperature for a specific duration (t_1 to t_2) During this period, the molecules are effectively "frozen" in their new orientation as the material cools down. After the application of the electric field, the high voltage is deactivated only when the material has been cooled back to room temperature. This step ensures that the oriented molecules retain their alignment even after the material returns to its solid state, thus locking in the enhanced nonlinear optical properties [49].

3. Theory

3.1. Second and Third harmonic generation (SHG&THG)

In linear optics, the propagation of light in a medium is governed by its dielectric properties, the response to the electromagnetic field, at the microscopic level, is expressed by the following polarization:

$$\vec{P} = \varepsilon_0 \chi^{(1)} \vec{E} \tag{1}$$

The term $\chi^{(1)}$ represents the linear susceptibility. It is directly related to the linear refractive index of the medium also causing the linear absorption and is the only not negligible term when the intensity of the electromagnetic wave is low.

In the last few centuries, nonlinear optics has experienced a renaissance due to lasers and the high fields that they produce, the response of the medium to such an excitation doesn't have the linear form anymore, and therefore it is now necessary to take into account other terms called nonlinear that appear in the following equation [50].

$$\vec{P} = \varepsilon_0 \left(\chi^{(1)} \vec{E} + \chi^{(2)} \vec{E}^2 + \chi^{(3)} \vec{E}^3 \ldots \right) \tag{2}$$

$$\vec{P} = \vec{P}_l + \vec{P}_{nl} \tag{3}$$

$\vec{P}_l = \varepsilon_0 \chi^{(1)} \vec{E}$: Linear polarization

$\vec{P}_{nl} = \chi^{(2)} \vec{E}^2 + \chi^{(3)} \vec{E}^3 \ldots$: Non-linear polarization

The terms $\chi^{(2)}$ and $\chi^{(3)}$ are the nonlinear susceptibilities of order two and three, respectively.

The second term $\chi^{(2)} \vec{E}^2$ Corresponds to the nonlinear optics producing effects of the second order effects such as the generation of the second harmonic. It depends strongly on the symmetry of the medium. The third term $\chi^{(3)} \vec{E}^3$ corresponds to nonlinear optics producing third-order effects. These effects are independent of the symmetry of the medium since they can occur even in mediums with a center of inversion. Examples are the generation of the third harmonic, Raman scattering, etc.

3.2. Theoretical models

3.2.1. Theoretical models to calculate the second-order nonlinear susceptibility

In order to measure the second-order nonlinear susceptibility $\chi^{(2)}$, many theoretical and computational research works have been developed. The nonlinear optical characterization is done by the SHG technique. Different theoretical models allow us to find the value of $\chi^{(2)}$ and also deal with different cases of materials, either in solution, thin film, powder, solid material, etc. Among these theoretical models are Lee's model, Jerpahrgnon and Kurtz's model, and Herman and Hayden's model.

The Jerphagnon and Kurtz model was developed in 1970. It considers that the second harmonic power induced by the propagation of a fundamental wave through a crystal of length L is given on the output side by the relation:

$$I_{2\omega} = I_M(\theta) \sin^2 \psi \tag{4}$$

$$\psi = \frac{\pi}{2} \frac{L}{L_C(\theta)} \tag{5}$$

ψ represents the interference factor between the free and bound waves, and Lc the coherence length depending on the angles θ_ω and $\theta_{2\omega}$.

The theoretical model of Herman and Hayden was developed in 1995 for the nonlinear optical characterization of bulk materials and thin films as well [51]. This model differs from those developed previously in that it has the advantage of expressing the second harmonic intensity by

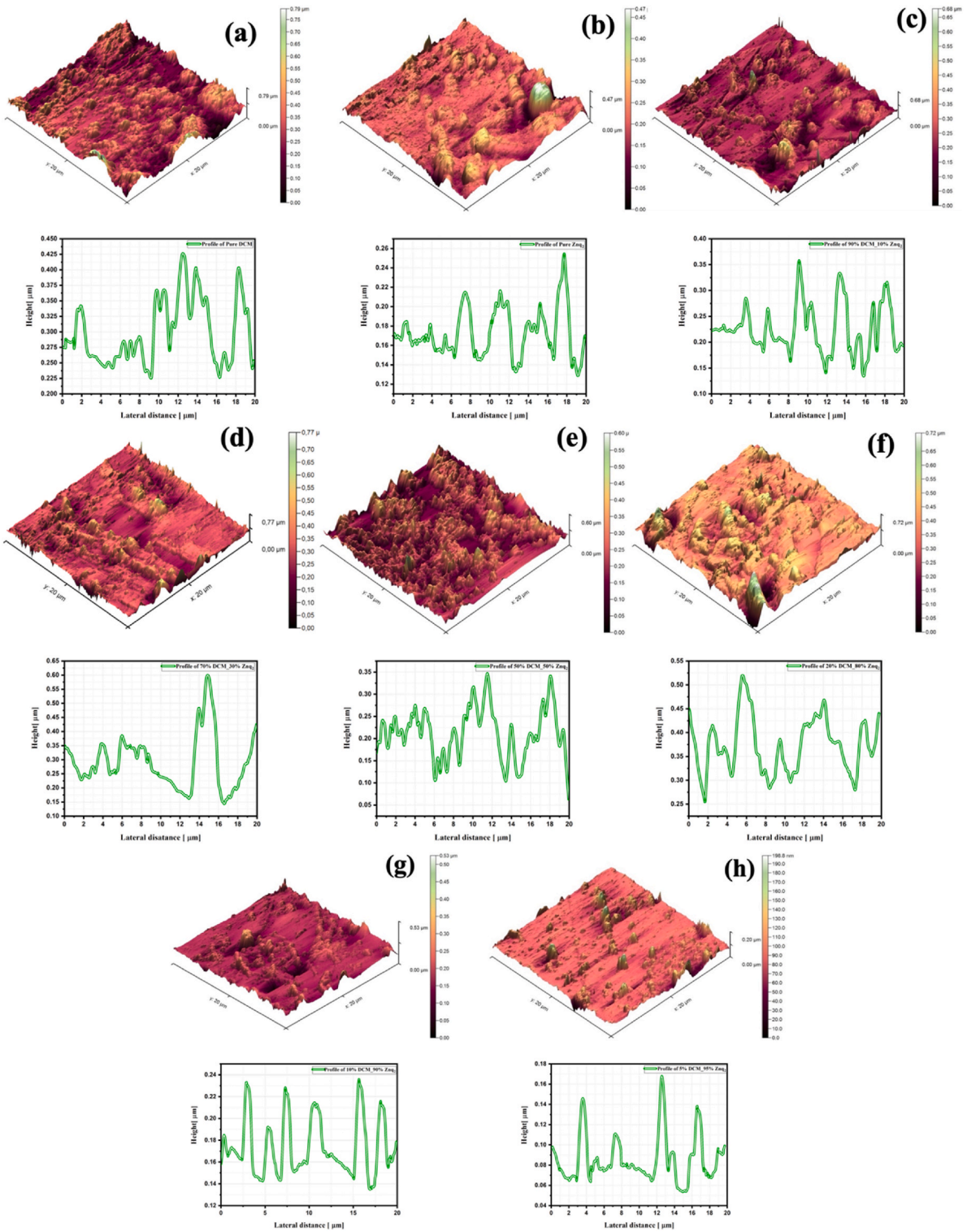


Fig. 4. 3D AFM image and profile of: (a)Pure DCM, (b) Pure Znq_2,(c)90%DCM_10%Znq_2,(d) 70%DCM_30%Znq_2,(e) 50%DCM_50%Znq_2,(f) 20%DCM_80%Znq_2,(g) 10%DCM_90%Znq_2,(h) 5%DCM_95%Znq_2.

taking into account the absorption of materials at the fundamental and second harmonic wavelengths.

In this work, the model used is the simplified Lee model [52,53]. This model is perfect for determining the second-order non-linear optical susceptibility of thin films. Its principle is based on the comparison of the macroscopic NLO properties of the studied sample with those of the reference material, in our case a quartz crystal slide of 0.5 mm thickness. This simplified model takes into account the thickness of the film d and the coherence length of quartz $l_{c,q}$:

$$\frac{\chi^{(2)}}{\chi_q^{(2)}} = \frac{2}{\pi}\frac{l_{c,q}}{d}\sqrt{\frac{I^{2\omega}}{I_q^{2\omega}}} \tag{6}$$

$\chi^{(2)}$ and $\chi_q^{(2)}$ are respectively the second-order nonlinear electrical susceptibilities of the material under study and the quartz. $I^{2\omega}$ and $I_q^{2\omega}$ respectively represent the maximum envelope intensities of the second

Table 1
RMS Roughness (Sq) and Mean Roughness (Sa) of the samples.

	RMS Roughness (Sq) [nm]	Mean Roughness (Sa)[nm]
Pure DCM	81,67	62,34
Pure Znq_2	44,75	30,03
90 % DCM_10%Znq_2	68	47
70%DCM_30%Znq_2	58,29	46,26
50%DCM_50%Znq_2	55,51	37,69
20%DCM_80%Znq_2	54,6	37,58
10%DCM_90Znq_2	26	16,63
5%DCM_95%Znq_2	12,91	7,64

harmonic signal of the material under study and the quartz.

It requires a reference material to normalize the amplitude of the bands obtained for the sample studied. The reference used is therefore quartz, with nonlinear susceptibility of order two is known and is worth ($\chi^{(2)} = 1$ p.m./V) [53,54].

The coherence length value is also given by the following expression:

$$l_{c,q} = \frac{\lambda_\omega}{4\left(n_{q(2\omega)} - n_{q(\omega)}\right)} \tag{7}$$

λ_ω is the wavelength of the fundamental beam ($\lambda_\omega = 1064$ nm), $n_{q(\omega)}$ and $n_{q(2\omega)}$ are the refractive indices of quartz at the wavelength of the beams, respectively, fundamental and second harmonic generated $n_{q(\omega)} = 1534$ at 1064 nm and $n_{q(2\omega)} = 1547$ at 532 nm).

3.2.2. *Theoretical models to calculate the third-order nonlinear susceptibility*

To measure the third-order nonlinear susceptibility $\chi^{(3)}$ the model of Kubodera and Kobayashi has been used [55]. This model has been developed taking into account two approaches, according to the absorption of the material or according to its negligence.The non-linear susceptibility of the third order is given in this case by the following formula:

$$\chi^{(3)} = \chi_s^{(3)}\left(\frac{2}{\pi}\right)\left(\frac{l_{s,c}}{l}\right)\left(\frac{I^{3\omega}}{I_s^{3\omega}}\right)^{1/2} \tag{8}$$

$$l_{s,c} = \frac{\lambda_\omega}{6\left(n_{q(3\omega)} - n_{q(\omega)}\right)} \tag{9}$$

$\chi_s^{(3)}$ represents the nonlinear susceptibilities of order three of silica, $I^{3\omega}$ is the maximum intensity of the envelope of the third harmonic signal of the studied material, $I_s^{3\omega}$ is the maximum intensity of the envelope of the third harmonic signal of silica, $l_{s,c}$ represents the silica coherence length and l the thickness of the sample.

At a wavelength of 1064 nm, the third-order nonlinear susceptibility of silica $\chi_s^{(3)} = 2 \times 10^{-22} m^2/V^2$ [56].

In general, this model directly compares the maximum amplitudes of the light intensities of the third harmonic of the medium to be studied with those of the reference material which is a sheet of fused silica SiO_2 of 1 mm thickness.

This equation is valid only in the case where the absorption of the material is low. In the opposite case, where the absorption becomes important, the relationship (8) is corrected by taking into account the magnitude related to the absorption.

$$\chi^{(3)} = \chi_s^{(3)}\left(\frac{2}{\pi}\right) l_{s,c}\left(\frac{\alpha/2}{1 - exp\left(-\alpha l/2\right)}\right)\left(\frac{I^{3\omega}}{I_s^{3\omega}}\right)^{1/2} \tag{10}$$

Where α refers to the linear absorption coefficient of the material at the fundamental wavelength.

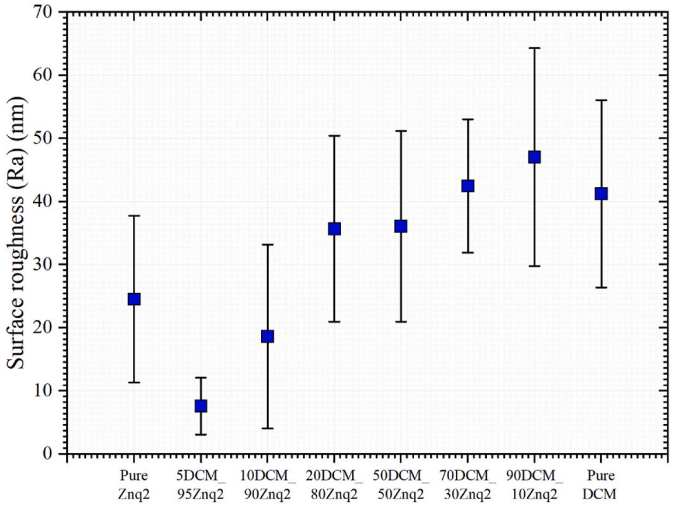


Fig. 5. AFM mean surface roughness (Ra), with standard deviation error bar, of different compositions of DCM co-doped Znq_2 films.

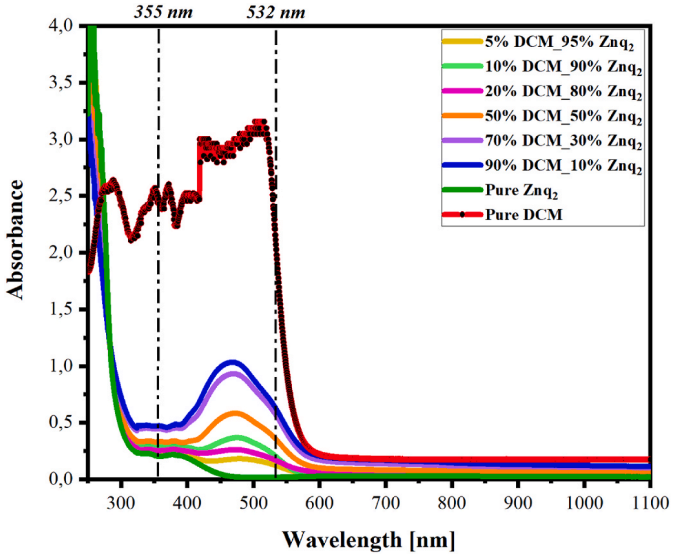


Fig. 6. UV–Vis absorption spectra of studied thin films.

4. Results and discussion

4.1. *Morphological properties*

Fig. 4 illustrates the 3D images (20 $\mu m \times$ 20 μm), profiles and roughness of the different samples. The roughness parameters, specifically RMS Roughness (Sq) and Mean Roughness (Sa), were obtained for different doping concentrations and are presented in Table 1.

The evaluation of the results indicates that the morphological properties of the samples have been influenced by doping. As shown in Table 1, the sample of pure DCM provided the largest roughness with a value of Sq = 81.67 nm. Whereas the sample with 5 % DCM represents the lowest Sq = 12,91 nm. The roughness of the other elements varies in an inversely proportional way to the variations of the percentages of DCM molecules in the films. The 3 D images of the samples demonstrate that the surfaces are inhomogeneous, and are characterized by the presence of islands of various dimensions depending on the sample.

To further validate the uniformity of the films, Fig. 5 depicting the surface roughness (Ra) with error bars provides a visual representation of the roughness variations across different samples. The error bars indicate the variability of roughness measurements, offering indirect

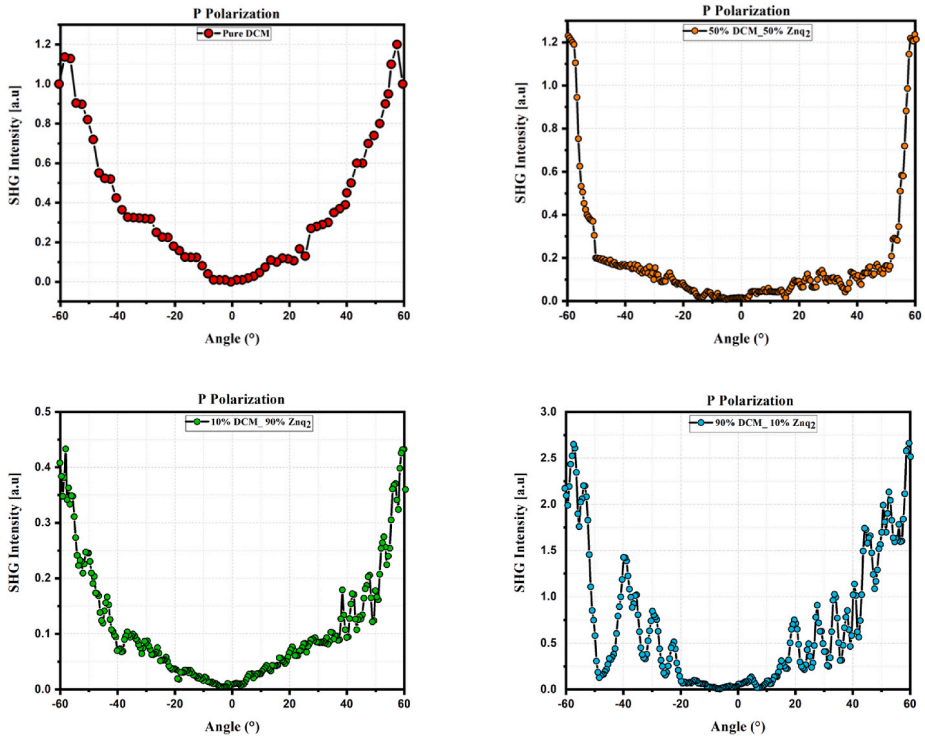


Fig. 7. Second harmonic intensity of DCM pure, Znq_2 pure, 10%DCM_90%Znq_2, 50%DCM_50%Znq_2, 90%DCM_10Znq_2 thin films and quartz as a function of the incident angle polarization P.
*DCM Pure: Second harmonic intensity for pure DCM thin films.
*Znq_2 Pure: Second harmonic intensity for pure Znq_2 thin films.
*10 % DCM - 90 % Znq_2: Intensity for a composite film with 10 % DCM and 90 % Znq_2.
*50 % DCM - 50 % Znq_2: Intensity for an equal mixture of DCM and Znq_2.
*90 % DCM - 10 % Znq_2: Intensity for a composite film with 90 % DCM and 10 % Znq_2.
*Quartz: Baseline second harmonic intensity for quartz.

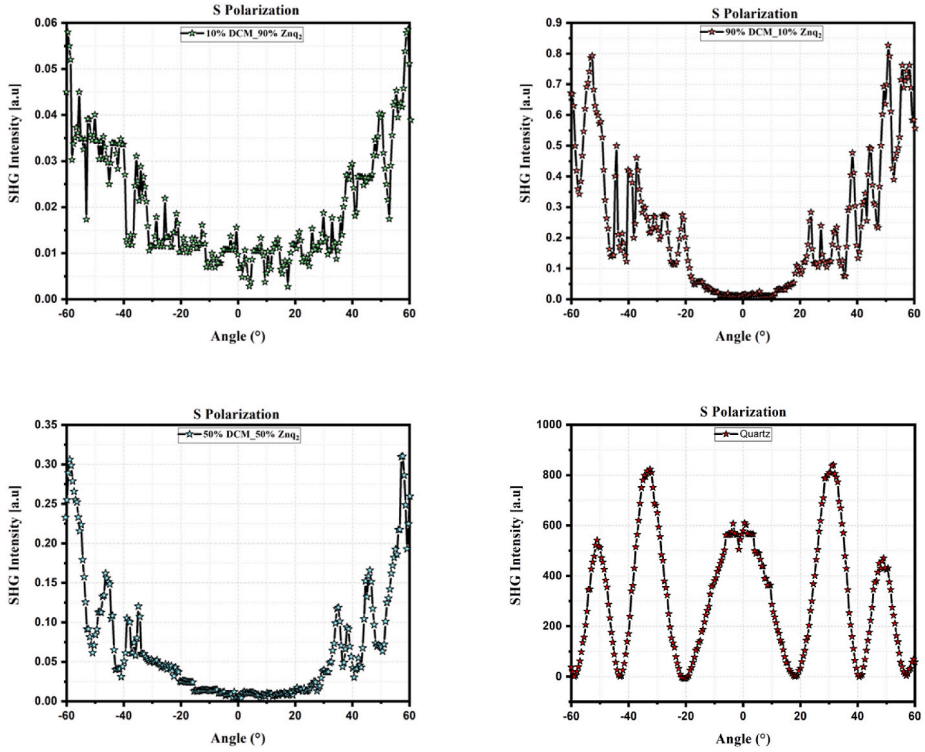


Fig. 8. Second harmonic intensity of DCM pure, Znq_2 pure, 10%DCM_90%Znq_2, 50%DCM_50%Znq_2, and 90%DCM_10Znq_2 thin films as a function of the incident angle polarization S.

Table 2
The values of the second-order nonlinear optical susceptibility χ(2) of thin films obtained from the second harmonic generation (THG) technique.

	d[nm]	$\alpha[10^3 cm^{-1}]$	$\chi^{(2)} pm.V^{-1}$	
			P	S
DCM	100	521.86	13.48	0
Znq_2	100	47.41	0	0
5 % DCM_95%Znq_2	100	30.09	3.05	1.07
10%DCM_90%Znq_2	100	49.02	3.38	1.32
20%DCM_80%Znq_2	100	41.18	4.2	2.34
50%DCM_50%Znq_2	100	84.86	6.30	3.19
70%DCM_30%Znq_2	100	124.67	7.5	4.2
90%DCM_10%Znq_2	100	149.3	10.34	6.07

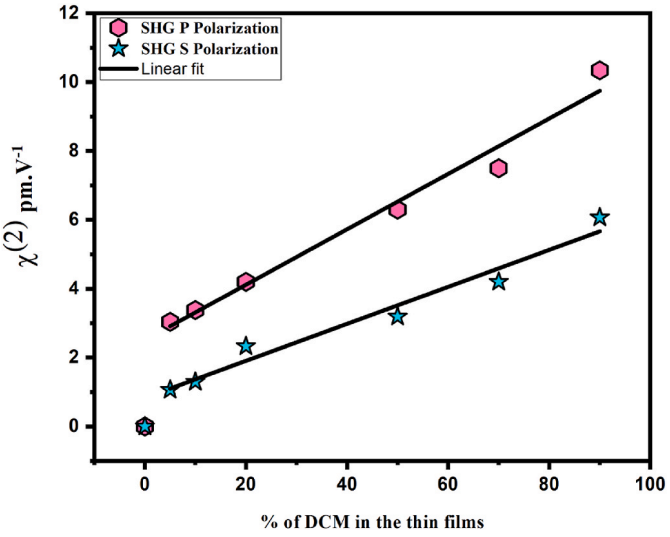


Fig. 9. The values of the second-order nonlinear optical susceptibility χ(2) of thin films as a function of the percentages of DCM in the thin films polarization P and S.

evidence of the uniformity of the samples. Notably, samples with higher Znq_2 content (and thus lower DCM content) not only exhibit lower roughness but also smaller error bars, suggesting improved uniformity, similar results were found by Ref. [57].

4.2. Linear optical measurements

The following illustration (Fig. 6) shows the absorption spectrum of thin films of pure DCM, pure Znq_2, and the samples with different compositions of Znq_2 and DCM with a thickness of 100 nm. The measurement was performed in the spectral range 190–1100 nm at normal incidence and room temperature. The sharp absorption peaks are centered around 510 nm for pure DCM, 467 nm for the other compositions, and 380 nm for pure Znq_2, respectively, which may be noticed in the absorption spectrum.

The bands could be attributed to the combination of the π→π* intraligand transition and ligand-metal charge transfer (LMCT). The analysis of the absorption spectra that the absorption band for the different compositions depends on the proportion of Znq_2 present in the structure and that the composition does not absorb at wavelengths of 1064 nm, which were used to study the second and third-order nonlinear optical properties (SHG and THG response). It is also noticed that the absorption for the wavelength corresponding to the generation of the second (532 nm) and third (355 nm) harmonics is several times lower in the case of DCM and Znq_2 composites compared to pure DCM. This makes the process of higher harmonics generation more effective even in the case of small amounts of Znq_2.

Table 3
The values of the third-order nonlinear optical susceptibility χ (3) of thin films obtained from the third harmonic generation (THG) technique for P polarization.

	d[nm]	$\alpha[10^3 cm^{-1}]$	$\chi^{(3)}.10^{-22} m^2.V^{-2}$
DCM	100	568.30	523
Znq_2	100	47.38	78.06
5 % DCM_95%Znq_2	100	53.05	106
10%DCM_90%Znq_2	100	67.27	111
20%DCM_80%Znq_2	100	58.83	122
50%DCM_50%Znq_2	100	76.94	184
70%DCM_30%Znq_2	100	103.49	212
90%DCM_10%Znq_2	100	109.50	250

4.3. Nonlinear optical measurements

4.3.1. SHG measurement

The second harmonic generation measurements of the studied samples were performed after the corona polarization technique. Figs. 7 and 8 illustrate the second harmonic intensity of the different samples as a function of polarization with incidence angles P and S. All measurements were performed directly after the corona polarization. The results presented by the figures have been obtained after the use of a filter to eliminate signal saturation.

The second-order nonlinear optical susceptibilities (SHG) were calculated from Lee's model. No SHG response was observed from the pure Znq_2 thin film, on the contrary, the other samples had a significant response, and a notable difference was found between the $\chi^{(2)}$ values as a function of the percentage of Znq_2 in the structure.

Table 2 represents the thickness of the studied samples, their absorption coefficients, and their third-order susceptibilities.

It can be observed that the values of the P-polarizations are more significant than those of the S-polarization. It is also noted that co-doping has influenced the measurements. Whereby increasing the percentage of Znq_2 in the structure decreases the effect of the nonlinearity for the samples, and the largest value is that of the pure DCM sample. As illustrated in Fig. 9, the second-order nonlinear susceptibility of the samples depends linearly on the percentage of DCM inside the thin film. Therefore, the main responsible element for the nonlinear effect is the DCM molecule.

4.3.2. THG measurements

There are different models used to determine third-order nonlinear susceptibility. The Kubodera-Kobayashi is suitable for determining the third harmonic generation results for our studied samples [58,59]. Using this model, we calculated the third-order nonlinear susceptibility presented in Table 3.

Fig. 10 represents the third harmonic intensity of pure DCM, pure Znq_2, 10%DCM_90%Znq_2, 50%DCM_50%Znq_2, 90%DCM_10Znq_2 thin films, glass, and silica as a function of the incident angle. The measurements were calculated for P and S polarization, the found results have equal value and are not dependent on the type of polarization.

As in the case of SHG measurements, THG measurements were also influenced by doping. Znq_2 thin film showed a typical response of quinoline materials such as Cuq_2, Mgq_2, and Alq_3 which have been previously reported in Ref. [22]. In this study, the non-linear response of Znq_2 is higher than in other published research. This can be attributed to certain reasons: The thickness of the thin films, the absorbance at 355 nm, the nature of the ligand-metal charge transfer, the electronegativity of the metal, and the shape of the orbitals, which are all important characteristics of this response, moreover, the non-linear optical response of Znq_2 is a result of the ligand-metal charge transfer (LMCT) [60,61]. While the DCM dye sample represented a very large third-order nonlinear response. This response can be attributed to the charge transfer inside the molecule [62,63].

For the other samples, the values of the third-order nonlinear optical

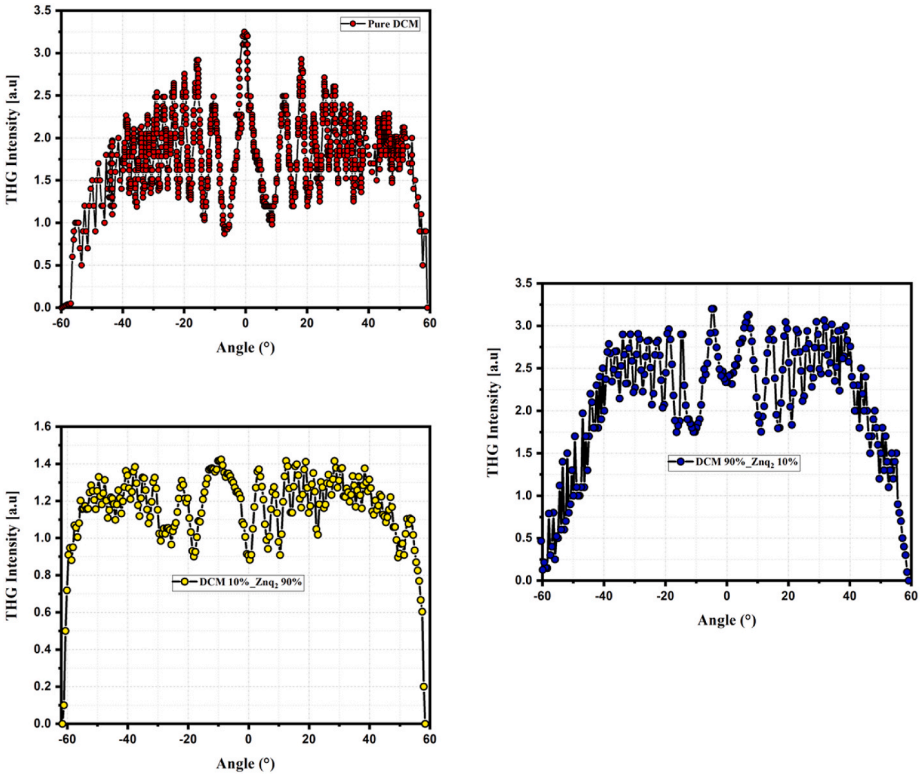


Fig. 10. Third harmonic intensity of pure DCM, pure Znq_2 pure, 10%DCM_90%Znq_2, 50%DCM_50%Znq_2, 90%DCM_10%Znq_2 thin films, Silica and Glass as a function of the incident angle.
*DCM Pure: Second harmonic intensity for pure DCM thin films.
*Znq_2 Pure: Second harmonic intensity for pure Znq_2 thin films.
*10 % DCM - 90 % Znq_2: Intensity for a composite film with 10 % DCM and 90 % Znq_2.
*50 % DCM - 50 % Znq_2: Intensity for an equal mixture of DCM and Znq_2.
*90 % DCM - 10 % Znq_2: Intensity for a composite film with 90 % DCM and 10 % Znq_2.
*Quartz: Baseline second harmonic intensity for quartz ….

susceptibility $\chi^{(3)}$ of the thin films varied approximately linearly as a function of the concentrations of DCM in the thin films polarized P, as shown in Fig. 11. Samples that contain a large percentage of DCM have high responses as a result of the dominance of the non-linearity of DCM in the sample.

5. Conclusions

In this work, the nonlinear optical properties and the morphological properties of thin films of the red dye DCM co-deposited with an organic semiconductor zinc complex (Znq_2) have been studied. The atomic force microscopy technique demonstrates a rough texture that is characterized by islands that vary in size and number. The samples were prepared with different compositions using the physical vapor deposition technique under a high vacuum. The second harmonic generation (SHG) and third harmonic generation (THG) of the samples were studied using Maker's fringe techniques. The second-order nonlinear susceptibilities of the different samples have been determined after the corona polarization techniques. The variation of the non-linearity of the samples was also discussed. The pure DCM sample exhibited the most significant nonlinear optical response, on the other hand, the pure Znq_2 thin film has no second harmonic response and its third harmonic response was smaller in comparison to the pure DCM sample. The signal of SHG and THG parameters of Znq_2 were influenced by the doping of with DCM, with a percentage of 5 % we could increase the third order response of pure Znq_2 samples from 78 $m^2.V^{-2}$ to 106 $m^2.V^{-2}$ and the second order response from 0 $pm.V^{-1}$ to 3.05 $pm.V^{-1}$ for P polarization and to 1.068 $pm.V^{-1}$ for S polarization. As a result, the doping of Znq_2 by DCM has influenced the morphological properties and has improved the second and third-order nonlinear properties. The significant nonlinear optical response of the prepared samples suggests that these systems may prove to be important candidates for a variety of photonic and optoelectronic applications.

CRediT authorship contribution statement

Amina Laouid: Writing – original draft, Software, Methodology, Investigation, Formal analysis, Data curation. **Houda El karout:** Funding acquisition, Formal analysis, Data curation. **Amine Alaoui Belghiti:** Visualization, Validation, Supervision, Methodology. **Krzysztof Wisniewski:** Validation, Supervision, Software, Formal analysis. **Przemysław Plociennik:** Validation, Software, Resources, Methodology, Investigation. **Youssef El kouari:** Investigation, Formal analysis, Conceptualization. **Bouchta Sahraoui:** Validation, Methodology, Investigation, Funding acquisition, Data curation. **Abdelowahed Hajjaji:** Writing – review & editing, Visualization, Validation, Supervision, Formal analysis. **Anna Zawadzka:** Writing – review & editing, Visualization, Validation, Supervision, Investigation.

Declaration of competing interest

The authors declare that they have no known competing financial interests or personal relationships that could have appeared to influence the work reported in this paper.

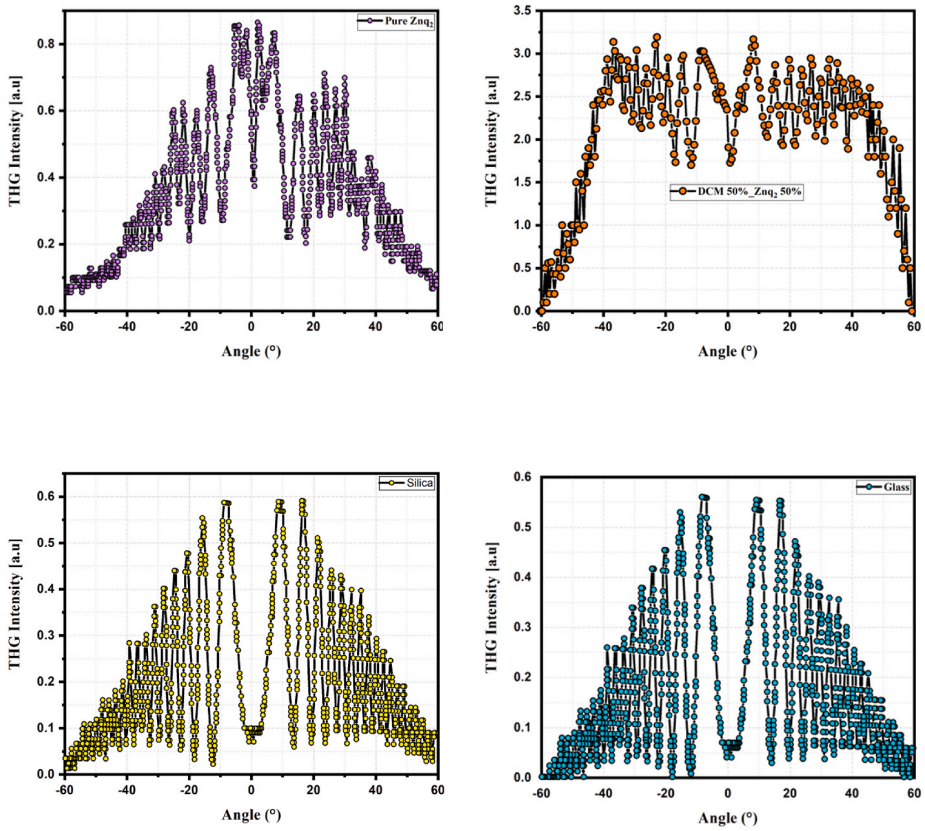


Fig. 10. (*continued*).

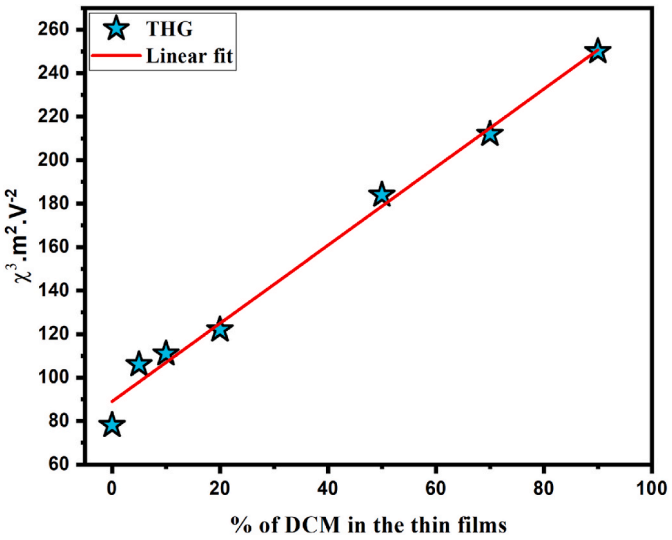


Fig. 11. The values of the third-order nonlinear optical susceptibility χ(3) THG of thin films as a function of the percentages of DCM in the thin films polarization P.

Data availability

Data will be made available on request.

Acknowledgments

This research has been financed from the funds of the Polish National Science Centre (grant no. 2017/25/B/ST7/02124). The films used in this paper were obtained using the Interdisciplinary Centre for Modern Technologies facilities, NCU, Torun, Poland. The research was carried out as part of the POLAND-FRANCE joint research projects POLONIUM NAWA (sygn. BPN/BFR/2021/1/00004) and IDUB project - emerging research fields: "Material Science and Technology".

References

[1] L. Tong, J.-X. Cheng, Label-free imaging through nonlinear optical signals, Mater. Today 14 (2011) 264–273, https://doi.org/10.1016/S1369-7021(11)70141-9.
[2] R. Abazari, E. Yazdani, M. Nadafan, A.M. Kirillov, J. Gao, A.M.Z. Slawin, et al., Third-order nonlinear optical behavior of an amide-tricarboxylate zinc(II) metal–organic framework with two-fold 3D+3D interpenetration, Inorg. Chem. 60 (2021) 9700–9708, https://doi.org/10.1021/acs.inorgchem.1c00997.
[3] R. Medishetty, K. Zaręba J, D. Mayer, M.A. Samoć, R. Fischer, Nonlinear optical properties, upconversion and lasing in metal–organic frameworks, Chem. Soc. Rev. 46 (2017) 4976–5004, https://doi.org/10.1039/C7CS00162B.
[4] P.P. Dey, A. Khare, Stoichiometry-dependent linear and nonlinear optical properties of PLD SiO x thin films, J. Alloys Compd. 706 (2017) 370–376, https://doi.org/10.1016/j.jallcom.2017.02.226.
[5] C. Liu, Y. Yuan, L. Cheng, J. Su, X. Zhang, X. Li, et al., Tunable nonlinear optical absorption in amorphous and crystalline Sb2Se3 thin films, J. Alloys Compd. 791 (2019) 753–760, https://doi.org/10.1016/j.jallcom.2019.03.295.
[6] I.D. Laktaev, B.M. Saidzhonov, R.B. Vasiliev, A.M. Smirnov, O.V. Butov, Second harmonic generation in colloidal CdSe/CdS nanoplatelets, Results Phys. 19 (2020) 103503, https://doi.org/10.1016/j.rinp.2020.103503.
[7] A. Zawadzka, K. Waszkowska, A. Karakas, P. Płóciennik, A. Korcala, K. Wisniewski, et al., Diagnostic and control of linear and nonlinear optical effects in selected self-assembled metallophthalocyanine chlorides nanostructures, Dyes Pigments 157 (2018) 151, https://doi.org/10.1016/j.dyepig.2018.04.048.
[8] A. Ahmadivand, B. Gerislioglu, Deep- and vacuum-ultraviolet metaphotonic light sources, Mater. Today 51 (2021) 208–221, https://doi.org/10.1016/j.mattod.2021.05.019.
[9] R. Ma, D.S. Sutherland, Y. Shi, Harmonic generation in transition metal dichalcogenides and their heterostructures, Mater. Today 50 (2021) 570–586, https://doi.org/10.1016/j.mattod.2021.07.023.
[10] L.M. Malard, T.V. Alencar, A.P.M. Barboza, K.F. Mak, AM de Paula, Imaging the crystal structure of few-layer two-dimensional crystals by optical nonlinearity. CLEO 2013 2013 Pap. JW2A05, Optica Publishing Group, 2013, p. JW2A.05, https://doi.org/10.1364/CLEO_AT.2013.JW2A.05.

[11] X. Miao, N. Xuan, Q. Liu, W. Wu, H. Liu, Z. Sun, et al., Optimizing nonlinear optical visibility of two-dimensional materials, ACS Appl. Mater. Interfaces 9 (2017) 34448–34455, https://doi.org/10.1021/acsami.7b09807.
[12] R.P.A. Emmanuele, M. Sich, O. Kyriienko, V. Shahnazaryan, F. Withers, A. Catanzaro, et al., Highly nonlinear trion-polaritons in a monolayer semiconductor, Nat. Commun. 11 (2020), https://doi.org/10.1038/s41467-020-17340-z.
[13] H.Y. Ramírez, J. Flórez, A.S. Camacho, Efficient control of coulomb enhanced second harmonic generation from excitonic transitions in quantum dot ensembles, Phys. Chem. Chem. Phys. 17 (2015) 23938–23946, https://doi.org/10.1039/c5cp03349g.
[14] L. Cheng, Y. Yuan, C. Liu, X. Cao, J. Su, X. Zhang, et al., Linear and nonlinear optical properties modulation of Sb2Te3/GeTe bilayer film as a promising saturable absorber, Results Phys. 13 (2019) 102282, https://doi.org/10.1016/j.rinp.2019.102282.
[15] Q. Chen, H. Zhang, Y. Feng, B. Miao, High polarizability enhanced EPR, optical linear & nonlinear and electric conductivity: role of NiFe2O4 nanocrystals in transparent tellurite glass-ceramics, J. Alloys Compd. 930 (2023) 167394, https://doi.org/10.1016/j.jallcom.2022.167394.
[16] K.D. Singer, S.J. Lalama, J.E. Sohn, Organic nonlinear optical materials, Integr. Opt. Circuit Eng. II 578 (1985) 130–136, https://doi.org/10.1117/12.950759. SPIE.
[17] C. Pintre I, J. Luis Serrano, M. Blanca Ros, J. Martínez-Perdiguero, I. Alonso, J. Ortega, et al., Bent-core liquid crystals in a route to efficient organic nonlinear optical materials, J. Mater. Chem. 20 (2010) 2965–2971, https://doi.org/10.1039/B923616C.
[18] B. Kulyk, D. Guichaoua, A. Ayadi, A. El-Ghayoury, B. Sahraoui, Metal-induced efficient enhancement of nonlinear optical response in conjugated azo-based iminopyridine complexes, Org. Electron. 36 (2016) 1–6, https://doi.org/10.1016/j.orgel.2016.05.028.
[19] D. Guichaoua, B. Kulyk, V. Smokal, A. Migalska-Zalas, O. Kharchenko, O. Krupka, et al., UV irradiation induce NLO modulation in photochromic styrylquinoline-based polymers: computational and experimental studies, Org. Electron. 66 (2019) 175–182, https://doi.org/10.1016/j.orgel.2018.12.022.
[20] M.B. Ros, Organic Materials for Nonlinear Optics, in: J.J. Novoa, D. Braga, L. Addadi (Eds.), Engineering of Crystalline Materials Properties. NATO Science for Peace and Security Series B: Physics and Biophysics, Springer, Dordrecht, 2008. https://doi.org/10.1007/978-1-4020-6823-2_18.
[21] S. Arroudj, A. Aamoum, L. Messaadia, A. Bouraiou, S. Bouacida, K. Bouchouit, et al., Effect of the complexation on the NLO electronic contribution in film based conjugated quinoline ligand, Phys. B Condens. Matter 516 (2017) 1–6, https://doi.org/10.1016/j.physb.2017.04.011.
[22] A. Popczyk, A. Aamoum, A. Migalska-Zalas, P. Płóciennik, A. Zawadzka, J. Mysliwiec, et al., Selected organometallic compounds for third order nonlinear optical application, Nanomaterials 9 (2019) 254, https://doi.org/10.3390/nano9020254.
[23] A. Laouid, A.A. Belghiti, K. Wisniewski, A. Hajjaji, B. Sahraoui, A. Zawadzka, Generation of red light with intense photoluminescence assisted by Forster resonance energy transfer from Znq2 and DCM thin films, Environ. Sci. Pollut. Res. 1–20 (2022), https://doi.org/10.1007/s11356-022-23217-z.
[24] R. Vivas-Reyes, F. Núñez-Zarur, E. Martínez, Electronic structure and reactivity analysis for a set of Zn-chelates with substituted 8-hydroxyquinoline ligands and their application in OLED, Org. Electron. 9 (2008) 625–634, https://doi.org/10.1016/j.orgel.2008.04.004.
[25] M. Lougdali, M. Zazoui, Y. Abboud, A.E. Bouari, A. Zawadzka, P. Płóciennik, et al., Linear and nonlinear optical properties of Manganese bis-(8- hydroxyquinoline) thin films for optoelectronic devices: experimental and computational studies, J. Mol. Struct. 1249 (2022) 131558, https://doi.org/10.1016/j.molstruc.2021.131558.
[26] M. Lougdali, Y. El kouari, M. Zazoui, Y. Abboud, A. Zawadzka, A. Migalska-Zalas, et al., Photoluminescence and nonlinear optical properties of Nickel bis-(8-hydroxyquinoline) thin film, Mater. Chem. Phys. 284 (2022) 126031, https://doi.org/10.1016/j.matchemphys.2022.126031.
[27] M. Lougdali, Y. El kouari, M. Zazoui, R. Anoua, Y. Abboud, A. Zawadzka, et al., Experimental and computational analysis of the Linear and Nonlinear optical properties of Magnesium bis-(8-hydroxyquinoline) thin film, J. Alloys Compd. 921 (2022) 165947, https://doi.org/10.1016/j.jallcom.2022.165947.
[28] P. Jiang, W. Zhu, Z. Gan, W. Huang, J. Li, H. Zeng, et al., Electron transport properties of an ethanol -soluble AlQ 3 -based coordination polymer and its applications in OLED devices, J. Mater. Chem. 19 (2009) 4551–4556, https://doi.org/10.1039/B904389F.
[29] N. Salah, A.S. Alshahrie, A. Saeed, Highly Efficient Organic Light Emitting Diode Based on Dysprosium Incorporated Tris-(8-Hydroxyquinoline) Aluminum, 2022. US11289664B1.
[30] A. Laouid, A. Alaoui Belghiti, K. Wisniewski, A. Hajjaji, A. Zawadzka, Structural and optical properties of DCM thin films prepared by PVD, Mater. Today Proc. (2022), https://doi.org/10.1016/j.matpr.2022.03.244.
[31] C.-W. Chang, Y.-T. Kao, E.W.-G. Diau, Fluorescence lifetime and nonradiative relaxation dynamics of DCM in nonpolar solvent, Chem. Phys. Lett. 374 (2003) 110–118, https://doi.org/10.1016/S0009-2614(03)00645-6.
[32] A. Szukalski, P. Krawczyk, B. Sahraoui, F. Rosińska, B. Jędrzejewska, A modified oxazolone dye dedicated to spectroscopy and optoelectronics, J. Org. Chem. 87 (2022) 7319–7332, https://doi.org/10.1021/acs.joc.2c00500.
[33] H. El Ouazzani, K. Iliopoulos, M. Pranaitis, O. Krupka, V. Smokal, A. Kolendo, et al., Second- and third-order nonlinearities of novel Push−Pull azobenzene polymers, J. Phys. Chem. B 115 (2011) 1944–1949, https://doi.org/10.1021/jp109936t.
[34] G. Noirbent, C. Pigot, T.-T. Bui, S. Péralta, M. Nechab, D. Gigmes, et al., Synthesis, optical and electrochemical properties of a series of push-pull dyes based on the 2-(3-cyano-4,5,5-trimethylfuran-2(5H)-ylidene)malononitrile (TCF) acceptor, Dyes Pigments 184 (2021) 108807, https://doi.org/10.1016/j.dyepig.2020.108807.
[35] A. Mohamed, Studying the optical properties of thin films prepared from polystyrene doped with DCM dye, Int. Lett. Chem. Phys. Astron. 61 (2015) 178–183. https://doi.org/10.18052/www.scipress.com/ILCPA.61.178.
[36] S. Wang, Z. Bian, X. Xia, C. Huang, Heterojunction organic solar cells based on donor-π-acceptor small molecule layers with controlled interface morphology, Org. Electron. 11 (2010) 1909–1915, https://doi.org/10.1016/j.orgel.2010.09.006.
[37] S. Hashimoto, R. Takagi, K. Okamura, A. Yabushita, T. Kobayashi, I. Iwakura, Ultrafast charge transfer dynamics in the excited state of DCM measured by a 6-fs UV pulse laser, Chem. Phys. 551 (2021) 111326, https://doi.org/10.1016/j.chemphys.2021.111326.
[38] K. Jung, Y. Kim, Theoretical studies of DCM derivatives with dual electron donating group, Mol Cryst Liq Cryst - MOL CRYST Liq CRYST 538 (2011) 45–52, https://doi.org/10.1080/15421406.2011.563629.
[39] M. Meyer, J.C. Mialocq, M. Rougée, Fluorescence lifetime measurements of the two isomers of the laser dye DCM, Chem. Phys. Lett. 150 (1988) 484–490, https://doi.org/10.1016/0009-2614(88)87235-X.
[40] H.-F. Lin, X.-X. Yang, S. Chen, Y.-R. Kang, J. Wang, Z.-Y. Jiang, et al., Controllable synthesis of multicolor Alq3:DCM single-crystalline microrods for optical waveguides, Org. Electron. 102 (2022) 106431, https://doi.org/10.1016/j.orgel.2022.106431.
[41] A. Zawadzka, A. Marjanowska, A. Laouid, K. Wisniewski, Y. El Kouari, P. Plociennik, Low-temperature influence on the properties and efficiency of thin-film perovskite solar cells fabricated by the PVco-D technique. https://doi.org/10.1016/j.solmat.2024.112993, 2024.
[42] I. El Ouedghiri-Idrissi, Z. Sofiani, A. Laouid, A. Talbi, A. Tarbi, Y. El Kouari, et al., Experimental and theoretical study on the optical and morphological properties of highly photoluminescent material 2,4,5-triphenyl imidazole, Opt. Quant. Electron. 56 (2024) 491, https://doi.org/10.1007/s11082-023-06186-6.
[43] M. Lougdali, Y. El Kouari, R. Anoua, M. Zazoui, I. El Oudghiri-Idrissi, Y. Abboud, et al., Study of photophysical properties of Cdq2 thin film, Mater. Today Proc. 66 (2022) 202–204, https://doi.org/10.1016/j.matpr.2022.04.485.
[44] R. Anoua, H. Lifi, S. Touhtouh, M. El Jouad, A. Hajjaji, M. Bakasse, et al., Optical and morphological properties of Curcuma longa dye for dye-sensitized solar cells, Environ. Sci. Pollut. Res. 28 (2021) 57860–57871, https://doi.org/10.1007/s11356-021-14551-9.
[45] B. Kulyk, A.P. Kerasidou, L. Soumahoro, C. Moussallem, F. Gohier, P. Frère, et al., Optimization and diagnostic of nonlinear optical features of π-conjugated benzodifuran-based derivatives, RSC Adv. 6 (2016) 14439–14447, https://doi.org/10.1039/C5RA25889H.
[46] A. Zawadzka, P. Płóciennik, J. Strzelecki, M. Pranaitis, S. Dabos-Seignon, B. Sahraoui, Structural and nonlinear optical properties of as-grown and annealed metallophthalocyanine thin films, Thin Solid Films 545 (2013) 429–437, https://doi.org/10.1016/j.tsf.2013.07.042.
[47] A. Nahata, J. Shan, J.T. Yardley, C. Wu, Electro-optic determination of the nonlinear-optical properties of a covalently functionalized Disperse Red 1 copolymer, JOSA B 10 (1993) 1553–1564, https://doi.org/10.1364/JOSAB.10.001553.
[48] M.A. Mortazavi, A. Knoesen, S.T. Kowel, B.G. Higgins, A. Dienes, Second-harmonic generation and absorption studies of polymer–dye films oriented by corona-onset poling at elevated temperatures, JOSA B 6 (1989) 733–741, https://doi.org/10.1364/JOSAB.6.000733.
[49] D.M. Burland, R.D. Miller, C.A. Walsh, Second-order nonlinearity in poled-polymer systems, Chem. Rev. 94 (1994) 31–75, https://doi.org/10.1021/cr00025a002.
[50] Boyd Nonlinear Optics, third ed..pdf n.d.
[51] W.N. Herman, L. Michael Hayden, Maker fringes revisited: second-harmonic generation from birefringent or absorbing materials, J. Opt. Soc. Am. B 12 (1995) 416–427, https://doi.org/10.1364/JOSAB.12.000416.
[52] G.J. Lee, S.W. Cha, S.J. Jeon, J.I. Jin, J.S. Yoon, Second-order nonlinear optical properties of unpoled bent molecules in powder and in vacuum-deposited film, J. Kor. Phys. Soc. 39 (2001) 912–915.
[53] N.V. Krishna, V.K. Singh, D. Swain, S.V. Rao, L. Giribabu, Optical, electrochemical, third order nonlinear optical, and excited state dynamics studies of bis(3,5-trifluoromethyl)phenyl-zinc phthalocyanine, RSC Adv. 5 (2015) 20810–20817, https://doi.org/10.1039/c4ra14390f.
[54] N. Mongwaketsi, S. Khamlich, M. Pranaitis, B. Sahraoui, F. Khammar, G. Garab, et al., Physical origin of third order non-linear optical response of porphyrin nanorods, Mater. Chem. Phys. 134 (2012) 646–650, https://doi.org/10.1016/j.matchemphys.2012.03.044.
[55] K. Kubodera, H. Kobayashi, Determination of third-order nonlinear optical susceptibilities for organic materials by third-harmonic generation, Mol Cryst Liq Cryst Inc Nonlinear Opt 182 (1990) 103–113, https://doi.org/10.1080/00268949008047792.
[56] F. Kajzar, Y. Okada-Shudo, C. Meritt, Z. Kafafi, Second- and third-order non-linear optical properties of multilayered structures and composites of C60 with electron donors, Synth. Met. 117 (2001) 189–193, https://doi.org/10.1016/S0379-6779(00)00498-7.
[57] A. Laouid, A. Alaoui Belghiti, K. Wisniewski, J. Strzelecki, A. Karakas, A. Gozutok, et al., Optical and morphological properties of DCM thin films co-doped of Znq2 by PVD: theoretical and experimental investigations, Vacuum 222 (2024) 112997, https://doi.org/10.1016/j.vacuum.2024.112997.

[58] T. Chtouki, Y. El Kouari, B. Kulyk, A. Louardi, A. Rmili, H. Erguig, et al., Spin-coated nickel doped cadmium sulfide thin films for third harmonic generation applications, J. Alloys Compd. 696 (2017) 1292–1297, https://doi.org/10.1016/j.jallcom.2016.12.089.

[59] B. Kulyk, B. Sahraoui, V. Figà, B. Turko, V. Rudyk, V. Kapustianyk, Influence of Ag, Cu dopants on the second and third harmonic response of ZnO films, J. Alloys Compd. 481 (2009) 819–825, https://doi.org/10.1016/j.jallcom.2009.03.117.

[60] C.C. Frazier, S. Guha, W.P. Chen, M.P. Cockerham, P.L. Porter, E.A. Chauchard, et al., Third-order optical non-linearity in metal-containing organic polymers, Polymer 28 (1987) 553–555, https://doi.org/10.1016/0032-3861(87)90468-X.

[61] H. Bozec, V. Guerchais, Molecular Organometallic Materials for Optics, Springer Science & Business Media, 2009.

[62] B. Derkowska, J.C. Mulatier, I. Fuks, B. Sahraoui, X.N. Phu, C. Andraud, Third-order optical nonlinearities in new octupolar molecules and their dipolar subunits, J. Opt. Soc. Am. B 18 (2001) 610, https://doi.org/10.1364/JOSAB.18.000610.

[63] N. Terkia-Derdra, R. Andreu, M. Sallé, E. Levillain, J. Orduna, J. Garín, et al., π conjugation across the tetrathiafulvalene core: synthesis of extended tetrathiafulvalene derivatives and theoretical analysis of their unusual electrochemical properties, Chem. Eur J. 6 (2000) 1199–1213, https://doi.org/10.1002/(SICI)1521-3765(20000403)6:7<1199::AID-CHEM1199>3.0.CO;2-G.